JGS
Journal of the Geological Society

Research article

https://doi.org/10.1144/jgs2024-264 | Vol. 182 | 2025 | jgs2024-264

The timing and significance of mid-crustal shearing and exhumation of amphibolite-facies rocks along the Great Glen Fault Zone, Scotland

Richard D. Law[1]*, J. Ryan Thigpen[2], Calvin A. Mako[1,3], Andrew Kylander-Clark[4], Mark J. Caddick[1], Lowell R. Moore[1], Cassandra Becker[1], Robert E. Holdsworth[5], Robin A. Strachan[6] and A. Graham Leslie[7]

[1] Department of Geosciences, Virginia Tech, Derring Hall, Blacksburg, VA 24061, USA
[2] Department of Earth and Environmental Sciences, University of Kentucky, 101 Slone Building, 121 Washington Avenue, Lexington, KY 40506, USA
[3] Arizona Geological Survey, 1955 East Sixth Street, Tucson, AZ 85721, USA
[4] Department of Earth Science, University of California, Santa Barbara, 1006 Webb Hall, Santa Barbara, CA 93106, USA
[5] Department of Earth Sciences, Durham University, Lower Mountjoy, South Road, Durham DH1 3LE, UK
[6] School of the Environment and Life Sciences, University of Portsmouth, Burnaby Building, Burnaby Road, Portsmouth PO1 3QL, UK
[7] British Geological Survey, Lyell Centre, Research Avenue South, Edinburgh EH14 4AP, UK

RDL, 0000-0001-6256-1944; JRT, 0000-0002-3075-5178; CAM, 0000-0002-0969-3080; AKC, 0000-0002-4034-644X; MJC, 0000-0001-8795-8438; REH, 0000-0002-3467-835X; RAS, 0000-0002-9568-0832; AGL, 0000-0003-1932-8420
* Correspondence: rdlaw@vt.edu

Abstract: The Rosemarkie Inlier lies on the NW side of the Great Glen Fault Zone (GGFZ) and is composed of foliated and lineated Archean orthogneisses and Moine metasedimentary rocks. The mylonitic foliation strikes NE–SW (parallel to the GGFZ), dips steeply SE and contains a gently to moderately plunging mineral lineation. Microstructural and quartz *c*-axis fabric analyses indicate that oblique sinistral shearing occurred under amphibolite-facies conditions. Laser ablation inductively coupled plasma mass spectrometry (LA-ICP-MS) analyses on monazite rims in the gneisses yielded $^{206}Pb/^{238}U$ ages of 401.8 ± 4.8 Ma (including 2σ uncertainty and a propagated additional 1% external uncertainty). Similar deformation and recrystallization temperatures indicated by quartz fabrics (610°C) and monazite–xenotime thermometry (616 ± 25°C), respectively, in the gneisses suggest that ductile sinistral shearing was ongoing at *c*. 402 Ma. The *c*. 402 Ma rim age is the youngest monazite age recorded in the Northern Highland Terrane (NHT) and indicates that sinistral shearing at mid-crustal levels was ongoing along the GGFZ in Lower Devonian (Emsian, 407–393 Ma) times when the thrust sheets of the NHT to the NW had already been exhumed. The Rosemarkie basement rocks are unconformably overlain by Middle Devonian (Eifelian, 393–387 Ma) sedimentary rocks, indicating time-averaged exhumation rates of *c*. 1.75 mm a^{-1} between 402 and *c*. 390 Ma, assuming a geothermal gradient of 30°C km^{-1}.

Supplementary material: Lasar-ablation split-stream data for Rosemarkie sample RM-22-08 are available at https://doi.org/10.6084/m9.figshare.c.7770211

Thematic collection: This article is part of the Exploring strain partitioning and kinematic evolution of the lithosphere: in honour of Micah Jessup collection available at: https://www.lyellcollection.org/topic/collections/exploring-strain-partitioning-and-kinematic-evolution-of-the-lithosphere

Received 27 November 2024; **revised** 21 March 2025; **accepted** 9 April 2025

The longevity of continental lithosphere means that once major faults or shear zones form, they are likely to persist unless there is pervasive restructuring of the lithosphere. It is well known that reactivated crustal-scale structures fundamentally influence the position and development of a broad range of features found throughout the geological record, including the location of many economic resources and seismic hazards. Where such structures are presently exposed cutting metamorphic basement, they typically display a long history of exhumation and preserve complex suites of fault-hosted deformation products – 'fault rocks' – that have formed at different depths and times in the crust (e.g. Sibson 1977; Holdsworth *et al.* 1997; Imber *et al.* 2001). The microstructures of these fault rocks can give an insight into the evolution of deformation mechanisms and the rheological behaviour of fault zones under a wide range of pressure and temperature conditions (e.g. Passchier and Trouw 2005 and references therein). The development of such fault rocks across a range of known pressure–temperature conditions is commonly associated with the growth of syntectonic mineral phases that can be dated using a range of geochronometers (Williams and Jercinovic 2002; Dumond *et al.* 2022; Moser *et al.* 2023; Ribeiro *et al.* 2023; Mottram and Cottle 2024; for application to fault zones in the Scottish Caledonides see Kemp *et al.* 2019; Holdsworth *et al.* 2020; Roberts and Holdsworth 2022). This provides direct absolute age constraints concerning the timing of fault rock deformation during reactivation and the associated history of exhumation.

The superimposed deformation that inevitably results from reactivation means that earlier formed fault rocks such as mylonites tend to be widely overprinted or excised by the effects of later brittle deformation, low-temperature metamorphism and fluid-related alteration (e.g. see Watts *et al.* 2007). As a result, earlier formed fault rocks tend to be subordinate features found in narrow fault-bounded slivers. These early relicts are important as they give insights into deeper crustal processes along reactivated faults/shear zones and also preserve the longest and most complete record of exhumation.

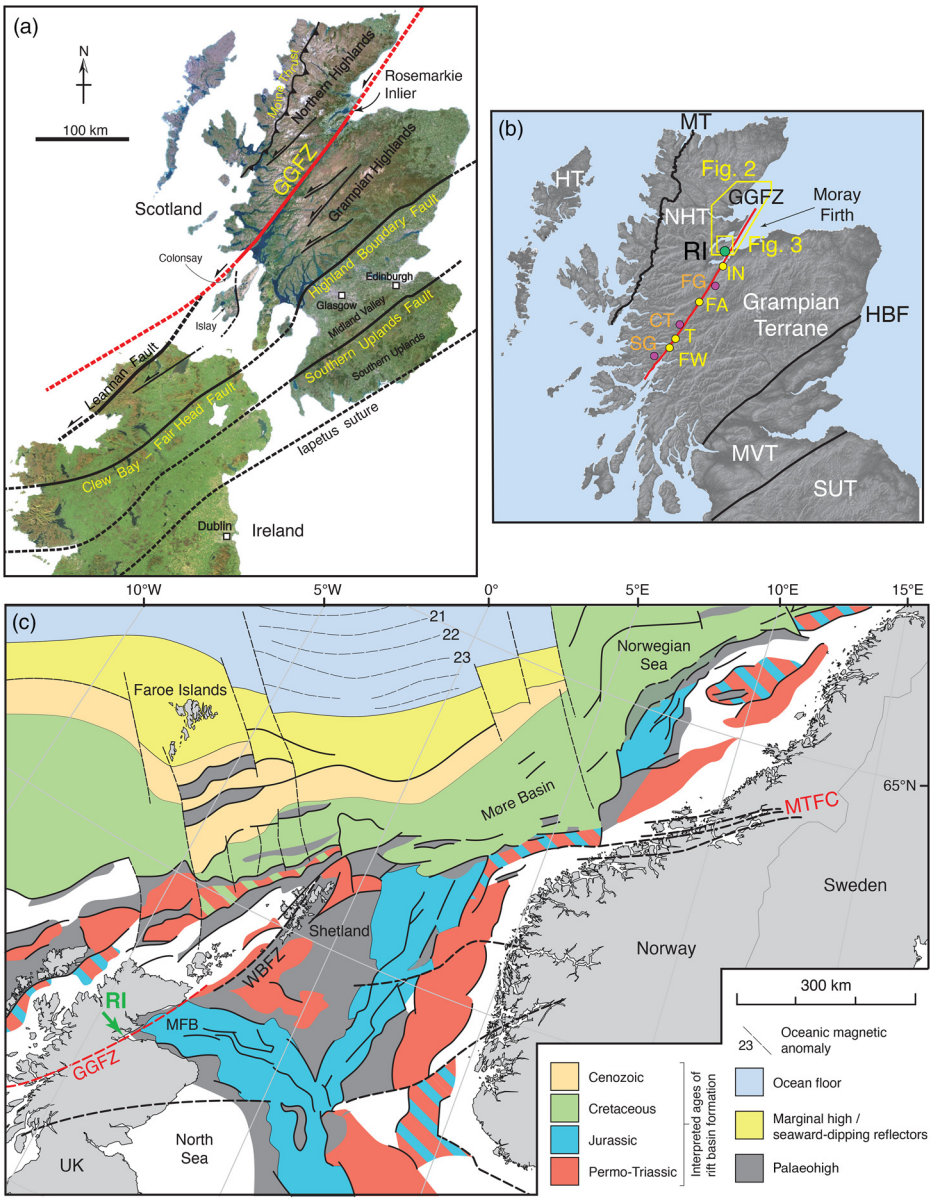

Fig. 1. (**a**) Major Caledonian faults in Scotland and Ireland and the location of the Rosemarkie Inlier on the NW side of the Great Glen Fault Zone (GGFZ). (**b**) Location of the Rosemarkie Inlier (RI) and positions of Figures 2 and 3. HT, Hebridean Terrane; NHT, Northern Highland Terrane; MVT, Midland Valley Terrane; SUT, Southern Uplands Terrane; MT Moine Thrust; HBF, Highland Boundary Fault; FA, Fort Augustus; FW, Fort William; I, Inverness; T, Torcastle; SG, Strontian Granite; CT, Clunes Tonalite; FG, Foyers Granite. (**c**) Map showing the location and regional context of the GGFZ in mainland Scotland with respect to the Walls Boundary Fault Zone (WBFZ) in Shetland and the Møre–Trøndelag Fault Complex (MTFC) in Norway, and their relationships to the major offshore basins of the NE Atlantic rifted margin. The left-hand column in the map legend refers to the interpreted age of the rift basin formation and not the age of the sediment fills; the position of the Rosemarkie Inlier (RI) on the NW side of the GGFZ is indicated; white offshore areas on the map indicate areas where no major rift basins are present. MFB, Moray Firth Basin. Source: (a) adapted from Prave *et al.* (2024); and (c) adapted from Watts *et al.* (2023).

The Great Glen Fault, also commonly referred to as the Great Glen Fault Zone (GGFZ), is one of Scotland's most significant crustal-scale faults (Fig. 1a, b) and is an important structure in the development of tectonic understanding globally – with 'demonstrably' large strike-slip displacements. Historically, it has provided a template for understanding other strike-slip fault zones around the world, and yet there has been rather limited study of its structural geology, the links between 'brittle' and 'ductile' structures, and its timing and relationship to sedimentation across the dying Caledonian Orogen. This is largely because outcrops along the GGFZ are sparse as the fault zone has been preferentially carved out by glaciation that has overdeepened the landscape – leaving tens of kilometre-scale waterbodies such as Loch Ness, Loch Lochy and Loch Linnhe. Previously published studies of fault rocks within the GGFZ have focused on the central part of the fault zone exposed around Torcastle and on the sides of the fault zone (mainly the SE side) between Fort Augustus and Fort William (Fig. 1b) (Stewart *et al.* 1997, 1999, 2000; Holdsworth *et al.* 2001; Becker 2023). Here exposed fault rocks are dominated by brittle microstructures with only occasional hints of earlier/deeper ductile/crystal plastic microstructures.

In this paper we examine coastal exposures of Precambrian basement rocks on the NW side of the GGFZ near Rosemarkie (Fig. 1b, c) where mid-crustal-level ductile microstructures associated with sinistral strike-slip shearing have locally escaped overprinting by later upper-crustal brittle structures, and the temperatures, crustal depths and timing of their formation can be constrained by petrochronology and microstructure/crystal fabric-based deformation thermometry. These basement rocks are unconformably overlain by Middle Devonian sedimentary rocks that allow us to estimate time-averaged exhumation rates during/following mid-crustal shearing on the GGFZ, with quartz and feldspar recrystallization microstructures tracking at least part of the cooling history during progressive exhumation.

Great Glen Fault Zone: Paleozoic structural evolution and tectonic setting

The NE-trending GGFZ is widely thought to have been initiated during the final stages of the Caledonian Orogeny in the late Silurian–early Devonian and has been periodically active throughout the Upper Paleozoic–Cenozoic (see summaries by Stewart *et al.* 1999; Mendum and Noble 2010; Le Breton *et al.* 2013; Dichiarante *et al.* 2020; Tamas *et al.* 2023). The GGFZ separates two terranes (Fig. 1a, b) that are thought to differ markedly in their Caledonian tectonic histories (see reviews by Law *et al.* 2024; Leslie *et al.*

2024). To the SE of the GGFZ, the Grampian Terrane (GT) is underlain by Dalradian Supergroup metasedimentary rocks (*c.* 800–517 Ma and possibly rocks as young as lowermost Ordovician at 470 Ma) that were pervasively deformed and metamorphosed during the Lower–Middle Ordovician-age Grampian phase of Caledonian orogenesis. To the NW of the GGFZ, the Northern Highland Terrane (NHT) is underlain mainly by Tonian (*c.* 1000–870 Ma) metasedimentary rocks with inliers of Archean–Paleoproterozoic basement gneisses. The former are part of the Moine Supergroup of Holdsworth *et al.* (1994) and are referred to informally in this contribution as 'Moine' (but see Krabbendam *et al.* 2022 for the revised terminology). The NHT was deformed and metamorphosed during both the Grampian and later Scandian (Silurian–lowermost Devonian) phases of Caledonian orogenesis. The latter has been attributed to the collision of Laurentia with Baltica during the final closure of the Iapetus Ocean. The apparent absence of the Scandian event in the Grampian Terrane has been taken to indicate a significant strike-slip offset (tens to hundreds of kilometres) on the GGFZ (e.g. Dewey and Strachan 2003; Prave *et al.* 2024).

To the SW, the GGFZ (e.g. Kennedy 1946; Holgate 1969; Smith and Watson 1983; Harris 1995) has been linked (Fig. 1a) with the Loch Gruinart–Leannan Fault in Islay and Ireland (Pitcher *et al.* 1964; Alsop 1992; Prave *et al.* 2024) and potentially, in pre-Atlantic opening reconstructions, to strike-slip faults of similar age in Newfoundland (Wilson 1962). To the NE, the GGFZ passes offshore into the Moray Firth (Fig. 1b), forming a major subvertical structure (e.g. Andrews *et al.* 1990). The fault can be traced for a further 23 km NE into deformed Mesozoic strata of the West Moray Firth Basin (Fig. 1c) (Bird *et al.* 1987; Underhill 1991; Thomson and Underhill 1993; Underhill and Brodie 1993). The GGFZ has also been linked with the Walls Boundary Fault (WBF) in Shetland (Fig. 1c) (Flinn 1961, 1992; McGeary 1989; McBride 1994; Watts *et al.* 2007; Dewey *et al.* 2015). Watts *et al.* (2007) highlighted the similarities in kinematic history of the two faults during the Paleozoic but also pointed to their significantly different post-Triassic histories (see also Armitage *et al.* 2021; Searle 2021). In Norway, the Møre–Trøndelag Fault Complex (MTFC) (Fig. 1c) was initiated as a sinistral shear zone at *c.* 405 Ma and may form part of the same network of late Caledonian faults (Sherlock *et al.* 2004; Fossen 2010; Watts *et al.* 2023).

Relationships between fault zone structures, dated igneous intrusions and post-orogenic sedimentary rocks constrain the main Caledonian sinistral displacement along the GGFZ to the period between *c.* 430 and *c.* 400 Ma (Stewart *et al.* 1999; but cf. Searle 2021). A component of Silurian displacement is indicated by the 428 Ma Clunes Tonalite that crops out on the NW side of the fault (Fig. 1b), and which was emplaced and sinistrally sheared while still in a submagmatic state (Stewart *et al.* 2001). Although the timing of sinistral motion on the GGFZ is relatively well constrained, the magnitude of early displacement is less certain because there is no unambiguous correlation of pre-Devonian features across the fault. Kennedy (1946) proposed a sinistral movement of *c.* 104 km; this was based on various lines of evidence, including the suggestion that the Strontian and Foyers granites (Fig. 1b) were once part of a single pluton that was displaced by the fault – an idea that has subsequently been discounted based on a range of structural, petrological and isotopic data (see the summary in Law *et al.* 2024). Winchester (1973) proposed a sinistral offset of 160 km based on the apparent offset of regional metamorphic zones across the fault. Piasecki *et al.* (1981) argued for a similar displacement based on the correlation of the Glenfinnan Group with the Central Highland Division gneisses (now referred to as the Badenoch Group) on the NW and SE sides of the fault, respectively; a correlation supported by more recent isotopic dating (Krabbendam *et al.* 2022; Strachan *et al.* 2024). Rather larger displacements are implied, however, by tectonic reconstructions that place the NHT adjacent to Baltica during the terminal Scandian collision, with late Silurian–Devonian sinistral displacements of at least 500 km along the GGFZ moving the Moine of the Northern Highland and Hebridean terranes into their present position with respect to the Dalradian of the Grampian Terrane (Dewey and Strachan 2003; Dewey *et al.* 2015; but cf. Searle 2021; Dewey and Ryan 2022). However, a more modest 250–300 km sinistral displacement along the GGFZ during the mid-Silurian–early Devonian might still permit a collision of NHT with Baltica (Prave *et al.* 2024).

On the Scottish mainland, the GGFZ comprises a *c.* 3 km-wide belt of fracturing and cataclasis of Moine and Dalradian protoliths. Fault rocks range from rare mylonite and quartz blastomylonite to cataclasite and phyllonite (Rathbone and Harris 1980; Stewart *et al.* 1997, 1999, 2000; Holdsworth *et al.* 2001; Mendum and Noble 2010). Semi-brittle shear zones cutting quartzites and psammitic and semi-pelitic gneisses in the mylonitic core of the fault zone exposed at Torcastle near Fort William (Fig. 1b) demonstrate a consistent sinistral sense of displacement with a minor southeasterly component of downthrow (Stewart *et al.* 1997, 1999, 2000; Stewart 2010). Chlorite and white mica growth in the shear zone fabrics imply shearing at depths equivalent to greenschist-facies metamorphism at crustal depths of 10–15 km (Stewart *et al.* 2000; Holdsworth *et al.* 2001). These semi-brittle shear zones cross-cut earlier microstructures, indicating dynamic recrystallization of quartz by subgrain rotation and minor grain-boundary migration (GBM) (accompanied by brittle deformation of feldspar). Associated quartz *c*-axis fabrics indicate oblique sinistral shearing (also with a SE component of downthrow) at deformation temperatures of *c.* 515°C (Becker 2023), corresponding to a crustal depth of 17 km, assuming a *c.* 30°C km^{-1} geotherm. The preservation of these mylonitic rocks in the core of the fault zone at Torcastle may reflect the presence of an exhumed positive flower structure formed during sinistral transpression (Stewart *et al.* 1999).

Devonian sedimentary rocks associated with the GGFZ are relatively undeformed compared with the metamorphic basement rocks (Stewart *et al.* 1999; Holdsworth *et al.* 2001; see also Mykura 1982; Stoker 1982). Post-Old Red Sandstone deformation structures along the fault zone are invariably brittle in style, and fault products are typically incohesive, comprising clay gouge and poorly consolidated breccia (May *et al.* 1997; Stewart *et al.* 1999). Outside of the fault zone, several studies of onshore Devonian basins in northern Scotland have highlighted the development of north–south-trending basin-bounding normal faults that are consistent with contemporaneous sinistral shear on the adjacent GGFZ (Wilson *et al.* 2010; Dichiarante *et al.* 2020).

Early Devonian shearing on the NW side of the GGFZ is recorded in the Rosemarkie Inlier exposed on the Black Isle (Figs 2 and 3), where Archean basement gneisses and Moine psammites intruded by 400–398 Ma granite veins (referred to as leucogranites by Mendum and Noble 2010) are all intensely deformed, with NE- and SW-plunging stretching lineations on steeply SE-dipping foliation planes (Figs 3b and 4) (Rathbone and Harris 1980; Highton 2009). Deformation microstructures and fabrics in the granite sheets and surrounding gneisses and psammites all indicate mid-crustal temperatures, although shearing in the granites was probably ongoing during cooling to wall-rock temperatures. The sheared basement rocks of the Rosemarkie Inlier are unconformably overlain by Middle Devonian conglomerates and sandstones (Figs 2 and 3) of middle–late Eifelian (*c.* 393–387 Ma) age (Rogers *et al.* 1989, fig. 2 – Cromarty & Nigg column; Marshall *et al.* 2007; Marshall 2024). Mendum and Noble (2010) argued that the basement rocks of the Rosemarkie Inlier were exhumed from mid-crustal depths during oblique sinistral shearing on the GGFZ.

The purposes of this paper are to provide: (1) additional microstructural, crystal fabric and petrochronological constraints

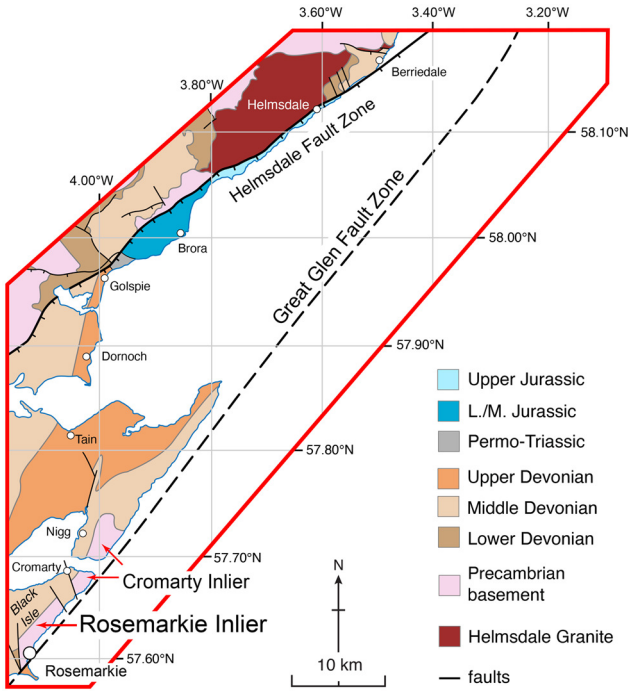

Fig. 2. Simplified regional geological map of the northwestern coast of the Inner Moray Firth Basin showing the positions of the Rosemarkie and Cromarty basement inliers and the unconformably overlying Devonian and Jurassic sedimentary rocks. Source: adapted from Tamas *et al.* (2023), with map positions of the Upper Devonian taken from Mendum and Noble (2010) and Marshall (2024).

on the kinematics, deformation temperatures, crustal depths and timing of shearing for the Rosemarkie Inlier; (2) an estimate of the time-averaged exhumation rate for the Inlier; and (3) to compare these datasets with available data from the NHT and recent/currently active strike-slip fault systems worldwide.

Rosemarkie Inlier: tectonic and structural setting

The Rosemarkie Inlier is one of two inliers of metasedimentary rocks exposed on the east coast of the Black Isle (Fig. 1b). These inliers mark the most southeastern positioned exposures of Archean basement and Moine rocks in mainland Scotland. The more northerly inlier, exposed on either side of the Cromarty Firth and usually referred to as the Cromarty Inlier, is dominantly composed of psammitic and semi-pelitic metasedimentary rocks that have provisionally been attributed to the Glenfinnan Group of the Moine (Rathbone and Harris 1980). In contrast, the Rosemarkie Inlier is composed of interlayered units of metasedimentary and meta-igneous rocks cut by variably deformed pink granite sheets, lenses and veins. U–Pb thermal ionization mass spectrometry (TIMS) zircon and monazite ages of 400.8 ± 2.6 and 397.6 ± 2.2 Ma, respectively, obtained from two granite samples (locations are shown in Fig. 4) by Mendum and Noble (2010) dated their emplacement as late Emsian (Lower Devonian). The psammites and semi-pelites may be of Moine affinity, whereas the feldspathic gneisses and particularly the amphibolites and hornblende-bearing gneisses exposed in the northern part of the inlier may be Archean basement (Horne 1923; Rathbone and Harris 1980; Highton 2009). Rathbone and Harris (1980) regarded the different rock types exposed in the Rosemarkie Inlier as indicating a tectonic interleaving of basement and Moine rocks, while Fletcher *et al.* (1996) considered it more likely that all of these rock types were of Moine affinity. However, U–Pb zircon dating of two hornblende–biotite felsic gneisses (Fig. 4) from the Rosemarkie Inlier (Mendum and Noble 2010) yielded Archean (2720–2930 Ma) protolith and Laxfordian (1745 Ma) recrystallization ages similar to those of many basement inliers of the NHT (Bird *et al.* 2023, fig. 3). Detrital zircons of Archean age are rare in undoubted Moine metasedimentary rocks in the NHT (Cawood *et al.* 2015), supporting the conclusion that at least the two gneisses sampled from the Rosemarkie Inlier are of basement affinity.

Horne (1923, p. 58) originally suggested that the amphibole-rich units (mainly exposed in the northern part of the Rosemarkie Inlier) may either be a fault-bounded slice of basement or a distinct group of Moine rocks 'brought up by the Great Glen Fault'. This interpretation was later expanded upon by Mendum and Noble (2010), who proposed that the basement inlier was extruded as a tectonic pip within a restraining bend on the GGFZ during oblique sinistral transpressional shearing on the fault zone in Lower Devonian times.

The Rosemarkie Inlier occupies the core of a NE–SW-trending antiformal structure, as indicated by bedding orientations in the surrounding Middle Devonian and Jurassic sedimentary rocks (Fig. 3a) (British Geological Survey 1958, 1973, 1997; Highton 2009; Mendum and Noble 2010). The basement rocks of the Rosemarkie Inlier are best exposed on an 8 km-long NE–SW-trending set of coastal outcrops located between high- and low-tide water levels and in adjacent cliffs (Fig. 3b). The basement rocks are unconformably overlain on their NW side by the Middle Devonian Kilmuir Conglomerate and Raddery Sandstone formations. Fletcher *et al.* (1996, table 1) listed these sedimentary units as being of Eifelian age (*c.* 393–387 Ma). Fossil pollen from this sequence (and correlation with the Achanarras Fish Bed of the Orcadian Basin) indicates that the basal beds were deposited in either the middle (Rogers *et al.* 1989) or late Eifelian (Marshall *et al.* 2007; Marshall 2024). Jurassic and Devonian rocks are downfaulted against basement rocks on the SE side of the antiform and exposed on the coastal section to the north of the Rosemarkie Inlier, with sheet dips of 15°–20° to the ESE (Le Breton *et al.* 2013). Conglomerates, sandstones and siltstones of interpreted Lower Devonian age, including the heavily tectonized Den Siltstone that may be of Emsian age (407–393 Ma: Fletcher *et al.* 1996, table 1), are downfaulted against the southwestern margin of the inlier (Fig. 3a).

Basement rocks in the southernmost part of the Rosemarkie Inlier are intensely fractured at the outcrop to hand-sample scale. These water-polished coastal exposures of intensely fractured basement rocks are the closest exposures to the brittle core of the GGFZ in the Moray Forth region (Figs 2 and 3a). In contrast, the basement rocks in the northern part of the inlier are much less intensely fractured (as recognized by Rathbone and Harris 1980), and grain-shape fabrics (foliation and lineation) defined by plastically deformed mineral grains (quartz, feldspar, amphibole and mica) are well preserved. Fractures in the northern part of the inlier are usually steeply dipping and are orientated either sub-parallel or at moderate–high angles to the NE-plunging grain-shape lineation. They range in scale from individual transgranular fractures observed in thin section to centimetre- to metre-scale zones of brecciation and mineral growth between clasts.

Deformation sequence recognized in the Rosemarkie Inlier

For the purposes of description, we have divided the coastal part of the Rosemarkie Inlier into the NE, Central and SW coastal sections (Fig. 3b). On published maps of the inlier (British Geological Survey 1958, 1973, 1997; Highton 2009; Mendum and Noble 2010), the dominant foliation (which will be referred to as S_2 below) strikes NE–SW in the NE section, ENE–WSW in the Central section, and almost north–south in the intensely fractured and relatively poorly exposed SW section. The NE section extends

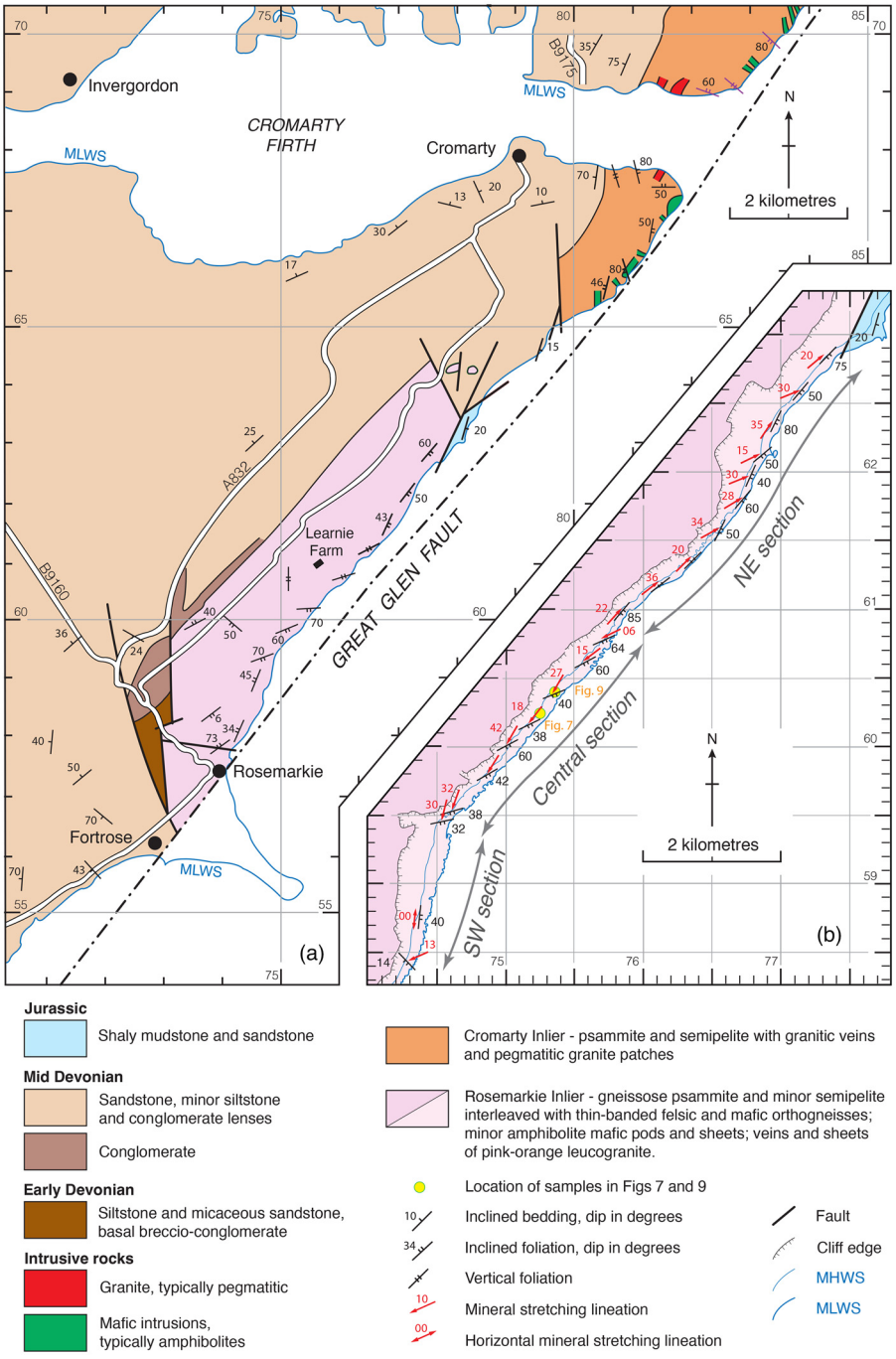

Fig. 3. (**a**) Geological map of the Rosemarkie and Cromarty inliers and the overlying/downfaulted Devonian and Jurassic sedimentary rocks. (**b**) Foliation and lineation data from the coastal exposures of the Rosemarkie Inlier. MHWS, mean high-water springs tide level; MLWS, mean low-water springs tide level. UK Ordnance Survey grid coordinates are indicated. Source: (a) adapted from Mendum and Noble (2010).

northeastwards from UK Ordnance Survey grid coordinate [NH 7600 6110] to [7735 6185], beyond which downfaulted Jurassic shales and sandstones are exposed. The Central section extends southwestwards from [NH 7600 6110] to [7455 5945], and the flat-lying water-worn exposures on the SW section extend almost due southwards from [NH 7455 5945] to [7400 5810].

Previously published structural (and isotopic) studies (Rathbone and Harris 1980; Mendum and Noble 2010; Stewart 2010) have focused exclusively on the NE section. However, structural mapping (foliations, lineations and folds) of the entire Rosemarkie Inlier coastal section at the 6 inch to the mile (1:10 560) scale was carried out by A.L. Harris in 1969 for the revised edition of the British Geological Survey (BGS) Sheet 94 (British Geological Survey 1973) and briefly reported on by Harris (1978). Clean copies of the original field slips covering our NE section and most of the Central section are curated at the BGS in Edinburgh, but field slips covering the SW area could not be located. Below we integrate a brief summary of our remapping of foliations and lineation in the NE and Central sections with previously published structural chronologies.

Rathbone and Harris (1980) recognized four deformation phases in the Rosemarkie Inlier, all of which formed under mid-crustal (amphibolite-facies) conditions and, as argued below, are of pre-Middle Devonian age. The principal planar fabric observed in all outcrops is a composite S_1/S_2 grain-shape foliation orientated parallel to compositional banding passing around the hinges of F_2 folds that presumably reflects the original bedding in the metasedimentary rocks. In the NE section, this foliation strikes NE–SW sub-parallel to the offshore trace of the Great Glen Fault and, where not deformed by later folds, has a steep dip to the SE (Figs 3b and 4). Tight to isoclinal folds observed in individual outcrops are attributed to D_2 (Mendum and Noble 2010). The S_1/S_2 foliation contains a strongly developed grain-shape lineation (L_2) that in the NE section plunges gently to moderately towards the NE

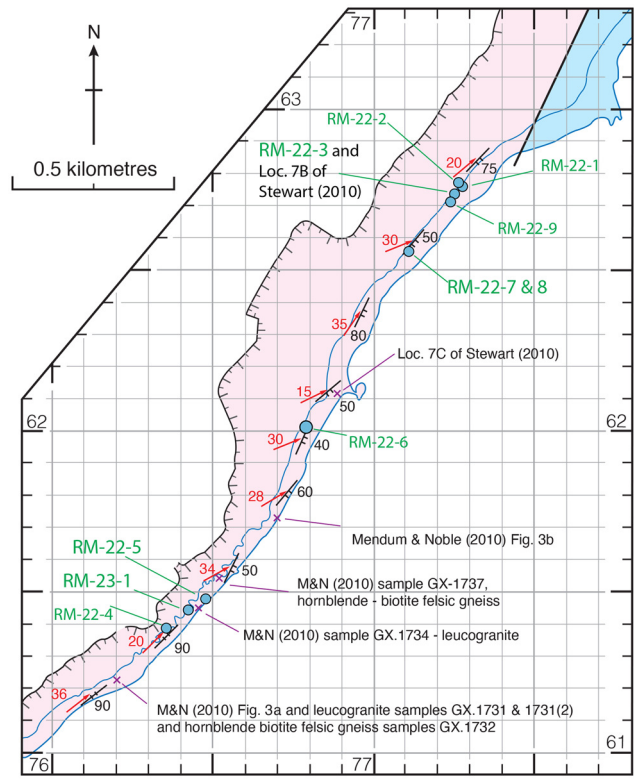

Fig. 4. NE section of the Rosemarkie Inlier showing the locations of samples for this study, together with the locations of granite and gneiss samples used by Mendum and Noble (2010) for isotopic dating, and exposures described in the field guide by Stewart (2010). Representative foliation and lineation data from Figure 3b are also shown.

to ENE (Figs 3b–6a). In contrast, in the Central section the composite S_1/S_2 foliation strikes ENE–WSW and dips steeply to the SSE, while the grain-shape lineation lying with the foliation plunges gently to moderately towards the SW to SSW (Figs 3b and 5). In the transition zone between the NE and Central sections the lineations are sub-horizontal to gently plunging. This transition in foliation and lineation orientation between the NE and Central sections is clearly shown in the 1969 field slips prepared for the BGS by A.L. Harris.

At some locations on the NE section of the inlier the S_1/S_2 foliation is folded about open to tight F_3 folds with subvertical hinge planes. According to Rathbone and Harris (1980) and Mendum and Noble (2010), the F_3 folds verge towards the SE and F_3 fold hinges plunge towards the NE to ENE, usually parallel to L_2 mineral lineations. F_4 folds also have subvertical hinge planes but verge towards the NW (Rathbone and Harris 1980). F_4 fold hinges also plunge towards the NE to ENE, parallel to L_2 mineral lineations. Folds hinges are much less commonly exposed in the Central section, where they consistently plunge towards the SW, sub-parallel to the local L_2 mineral lineation.

Numerous veins, lenses and sheets of red-pink microgranite and granitic pegmatite cut the metamorphic rocks in the NE section of the Rosemarkie Inlier. As noted above, Mendum and Noble (2010) refer to all these intrusions as leucogranites. They occur as sharply bounded steeply dipping intrusions that range in thickness from less than 1 cm up to 5 m and are usually concordant or subconcordant to the NE–SW-striking S_1/S_2 grain-shape foliation (Fig. 6b). In a few outcrops these intrusive bodies cut across the S_1/S_2 grain-shape foliation (Highton 2009). They frequently display 'pinch-and-swell' boudinage structures in gently dipping NE–SW-trending strike-parallel exposures and, less commonly, in steeply dipping NW–SE-trending dip-parallel exposures. The granites are commonly pervasively sheared and contain internal grain-shape fabrics (Fig. 6c–f) that are typically parallel to the margins of the NE–SW-striking planar sheets, with a subhorizontal (NE–SW-trending) to gently plunging mineral lineation on both the internal foliation (Fig. 6d) and the margins of the intrusions.

Analytical methods

A suite of orientated samples was collected from the NE section of the inlier (Fig. 4) for kinematic, deformation temperature and isotopic dating studies. All samples were examined in polished slabs and thin sections were cut perpendicular to foliation and parallel to lineation (*XZ* sections).

Microstructures and quartz *c*-axis fabrics

Microstructures were imaged using an optical microscope. Quartz *c*-axis fabrics were measured using an optical microscope and Leitz universal stage, with 1000 grains being measured in each sample. Fabrics are displayed on lower-hemisphere, equal-area projections. For the purposes of description, all reported microstructures and fabrics are viewed geographically downwards onto the NE-striking *XZ* section plane in which lineation plunges gently to moderately towards the NE. In this reference frame, oblique sinistral shearing (with a NW side up to the SW and a SE side down to the NE sense of motion) would be indicated by a sinistral shear sense, while oblique dextral shearing (with a NW side down to the NE and a SE side up to

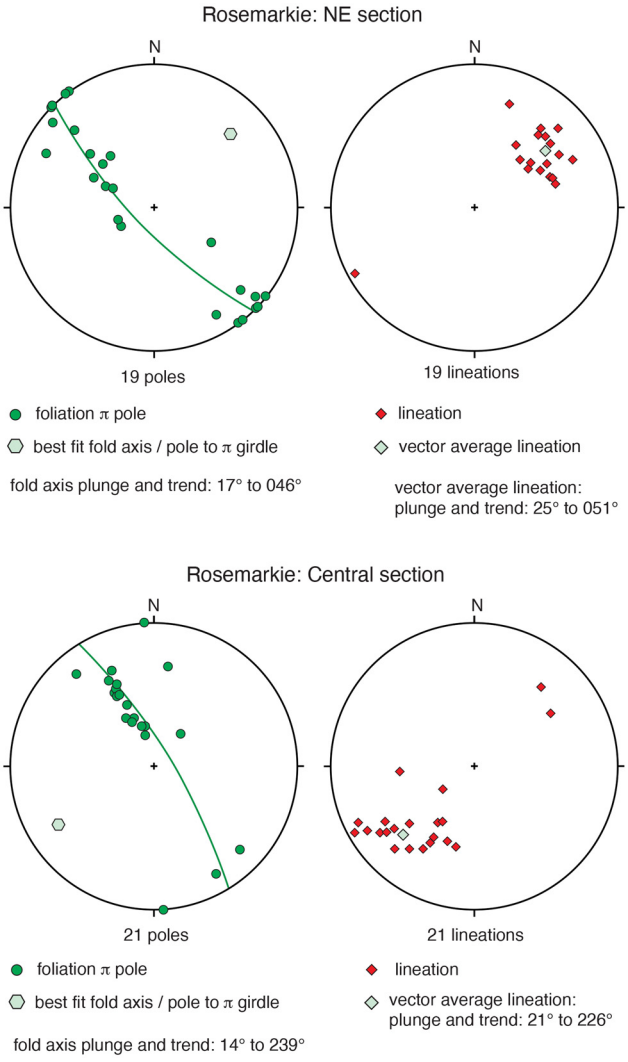

Fig. 5. Foliation and lineation data for the NE and Central sections of the Rosemarkie Inlier. Lower-hemisphere, equal-angle plots.

Fig. 6. Gneisses and granites from the NE section of the Rosemarkie Inlier; map positions are indicated in Figure 4. (**a**) Outcrop of foliated and lineated gneisses from which samples RM-22-07 and RM-22-08 were collected; the orientation of the foliation and lineation are indicated. (**b**) Vertical 1 m-wide NE–SW-striking pink granite injected parallel to foliation in the surrounding gneisses; Mendum and Noble (2010) granite samples GX.1731, GX1731 (2) and gneiss sample GX.1732 are from this area. (**c**)–(**f**) Porphyritic NE–SW-striking and steeply SE-dipping granite sheet from which sample RM-22-03 was collected; the intrusion was originally described by Stewart (2010, location 14.7B). (c) Horizontal erosion surface orientated almost perpendicular to foliation and at a low angle to the gently NE-plunging lineation; the grain-shape foliation is defined by plastically deformed quartz ribbons that anastomose around equant to slightly elongate feldspar porphyroclasts; note the variable size of the white feldspar clasts, smaller clasts may be fragments of original larger feldspar porphyroclasts. (d)–(f) Horizontally cut surfaces in sample RM-23-03 viewed vertically downwards. (d) The orientation of the foliation and grain-shape lineation on the foliation are indicated. (e) A shear band oblique to foliation indicating a sinistral shear sense. (f) Sigma-shaped wings of quartz and feldspar on an elongate white feldspar porphyroclast indicating a sinistral shear sense.

the SW sense of motion) would be indicated by a dextral shear sense.

Electron probe microanalysis

Element maps of monazite and xenotime were collected on a JEOL JXA-iHP200F electron microprobe at Virginia Tech, using a 200 nA beam current and 15 kV accelerating voltage. The pixel dwell time was 50 ms, with multiple acquisitions employed for some monazite crystals. Ca, Ce, Th, Y and Si were analysed using wavelength-dispersive spectrometry (WDS) (utilizing pentaerythritol (PET), lithium fluoride (LiF) and thallium acid phthalate (TAP) diffracting crystals). Maps of additional elements, mostly used to provide spatial context, were collected on a solid-state energy dispersive spectrometer.

Laser-ablation split-stream mass spectrometry

U–Pb isotope and trace element analysis of monazite and xenotime was performed at the University of California, Santa Barbara, following the methods outlined in Kylander-Clark *et al.* (2013) and Kylander-Clark (2017). The laser-ablation split-stream (LASS) system combines a Photon Machines 193 nm ArF Excimer laser, equipped with a Hel-Ex ablation cell, with a Nu Instruments HR Plasma high-resolution multicollector inductively coupled plasma mass spectrometry (MC-ICP-MS) system for collecting U–Pb isotope data, and an Agilent 7700 quadrupole ICP-MS for determining trace element concentrations. The laser parameters for analysis consisted of an 8 μm spot ablated at *c.* 1 J cm^{-2} and 3 Hz for 12 s, following a 20 s baseline and two-shot pre-ablation. Unknowns were bracketed by monazite reference material (RM) 44069 (Aleinikoff *et al.* 2006); the reference materials Bananiera (Palin *et al.* 2013; Horstwood *et al.* 2016), Trebilcock (Tomascak *et al.* 1996) and FC1 (monazite and xenotime: Horstwood *et al.* 2016) were analysed periodically for quality control and yielded average ages within 2% of their accepted values. For element concentrations, ^{31}P was used as the internal standard, assuming 12.9 wt% for monazite and 15.2 wt% for xenotime, and Bananeira was used as the reference material. Raw U–Pb isotope and trace element data were reduced using Iolite v3 software (Paton *et al.* 2010) to correct for instrument drift, laser-ablation-induced downhole elemental fractionation, plasma-induced elemental fractionation and instrumental mass bias.

Shear-sense indicators and deformation temperatures in the NE section of the Rosemarkie Inlier

Deformation temperatures and shear senses were estimated using microstructures and quartz *c*-axis fabrics. Macroscopic shear-sense indicators are extremely rare in deformed gneisses, psammites and amphibolites but are at least locally developed in some of the granite intrusions. It is likely that because of this, with the exception of the granites (Stewart 2010), shear-sense indicators have not been

mentioned in previous descriptions of the inlier (Rathbone and Harris 1980; Highton 2009; Mendum and Noble 2010).

Microstructures

In the gneisses and psammites, both quartz and feldspar have deformed plastically, although quartz is far less abundant than feldspar. The grain-shape foliation is defined by elongate to ribbon-like domains of recrystallized quartz and feldspar (Fig. 7), with the two minerals usually forming separate ribbons, and often separated by elongate white mica grains. In areas where feldspar (both orthoclase and plagioclase) and quartz grains occur next to each other (including samples RM-22-07 and RM-22-05) boundaries between adjacent feldspar and quartz grains are sinuous to lobate with gently curving grain-boundary segments (Fig. 8a–c) often measuring more than 50–100 μm in length, indicating recrystallization by high-temperature GBM in both feldspar and quartz grains. Tapering deformation twins are present in some of the plagioclase grains (Fig. 8a, b), and internally both quartz and feldspar grains display a range of microstructures (undulatory extinction, tilt walls and, locally, blocky extinction) that also indicate high-temperature deformation. Myrmekites are widespread. Crystal-plastic deformation of feldspar by dislocation creep (as is indicated by these microstructures) is only observed in naturally deformed rocks deformed under upper-amphibolite (*c*. 600–700°C) or higher conditions (see the review by Tullis 2002). Fazio *et al.* (2020) estimated a minimum temperature of *c*. 675°C for the onset of GBM recrystallization of feldspar. Relatively high deformation temperatures are also indicated by brick-red highly pleochroic and unaltered biotite grains in some of the Rosemarkie gneiss and psammite samples (e.g. sample RM-22-08), which are candidates for future Ti-in-biotite thermometry. In fault rock terms, these rocks are mylonitic to blastomylonitic (Sibson 1977; but see discussions by Schmid and Handy 1991 and Snoke and Tullis 1998 on the difficulty of applying these terms at high metamorphic grades when grain boundaries are highly mobile).

Minimum temperatures for the onset of recrystallization by GBM in quartz are usually assumed to be in the range of *c*. 490–530°C (see the review by Law 2014). However, although the majority of microstructures such as large-scale (hundreds of micrometres) gently curving quartz and feldspar grain boundaries in samples RM-22-05 and RM-22-07 indicate recrystallization by high-temperature GBM, much smaller (20–40 μm) and localized bulges between adjacent feldspar and quartz grains in sample RM-22-05 indicate later and lower temperatures of at least incipient recrystallization of feldspar and quartz by grain-boundary bulging (GBB), probably within the temperature ranges of 450–550°C for feldspar (Passchier and Trouw 2005, p. 260; Fazio *et al.* 2020) and 300–400°C for quartz (see the review by Law 2014). Similar microstructures are seen in sample RM-23-01, a sheared quartz vein located on the margin of a foliation parallel granite sheet. In this sheared quartz vein 'island', quartz grains indicating high-temperature GBM coexist with an order of magnitude smaller grain-boundary bulges between adjacent quartz grains (Fig. 8g, h), indicating relatively low-temperature (300–400°C) GBB recrystallization of quartz. This all suggests that a range of feldspar and quartz microstructures have been 'frozen in' during the cooling and exhumation of the Rosemarkie rocks.

In gneiss sample RM-22-07, the plastically deforming quartz–feldspar ribbons anastomose around larger (3–5 mm) feldspar grains, which appear to have remained relatively rigid and preserve microstructural evidence for potential sinistral shear. Asymmetrical development of myrmekite patches referred to as 'quarter structures' (see the review by Passchier and Trouw 2005, p. 150) on the edges of one of the largest rhomb-like orthoclase grains in this sample also suggests a sinistral shear sense. This shear sense is unequivocally confirmed by large (2–5 mm) asymmetrical white mica fish in the same sample (Fig. 8d, e) using the geometrical criteria reviewed by ten Grotenhuis *et al.* (2003) and Passchier and Trouw (2005, p. 142).

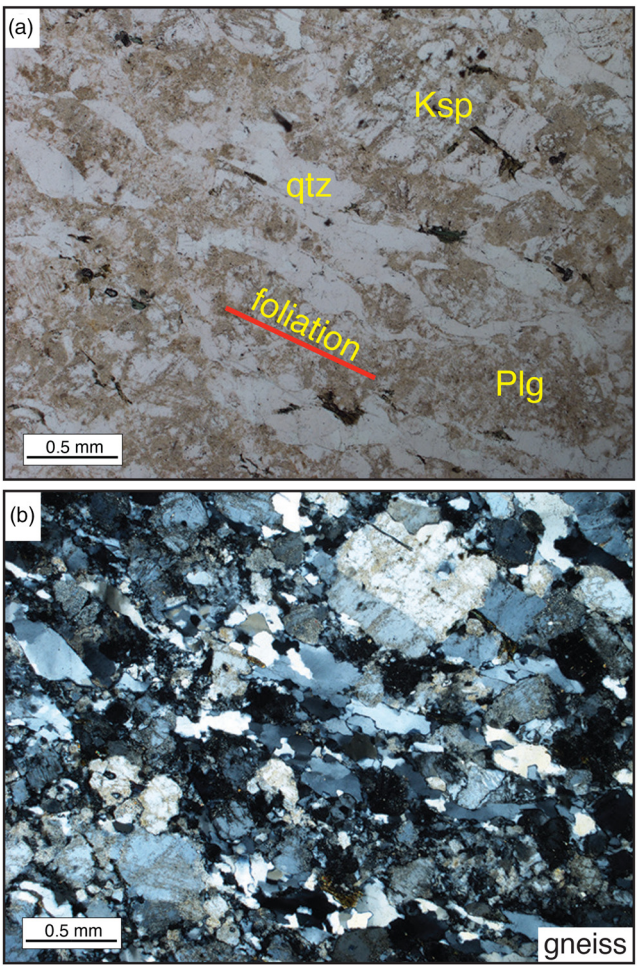

Fig. 7. Photomicrograph pair taken in (**a**) plane-polarized light and (**b**) cross-polarized light illustrating a typical grain-shape foliation in the sheared/mylonitic gneisses (the location is shown in Fig. 3b) defined by elongate to ribbon-like domains of recrystallized quartz and feldspar. Ksp, orthoclase feldspar; Plag, plagioclase feldspar; qtz, quartz.

Numerous amphibolites and amphibole-rich gneisses (samples RM-22-01, RM-22-02, RM-22-04, RM-22-06 and RM-22-09) are exposed in the NE section of the Rosemarkie Inlier (Fig. 4), and are composed of elongate laths of amphibole interlayered with recrystallized feldspar (plagioclase and orthoclase) and variable (but always very minor) amounts of quartz. This interlayering of amphibole and feldspar defines the grain-shape foliation in the gneisses (Fig. 8f). The amphibole laths range from 2 to 4 mm in length and from 0.3 to 0.5 mm in width. In some foliation-parallel domains the amphibole laths have a shattered' appearance due to localized brittle shearing, but no obvious chemical retrogression is observed. Plagioclase and orthoclase grains are equant to elongate in outline. The plagioclase grains often display undulose extinction and tapering deformation twins, indicating that they have deformed plastically. Grain-boundary microstructures between adjacent feldspar grains suggest that they have been recrystallized by GBM. No convincing microstructural shear-sense indicators were found in any of these amphibole-rich gneisses. Planar extensional fractures orientated at a high angle to foliation (and lineation) with no obvious fracture-parallel offset of the grain-shape foliation were recorded in thin sections from several of the amphibole-rich gneisses (Fig. 8f).

Granite sample RM-22-03 was collected from a NE–SW-striking and steeply SE-dipping granite sheet at the northern of the NE section

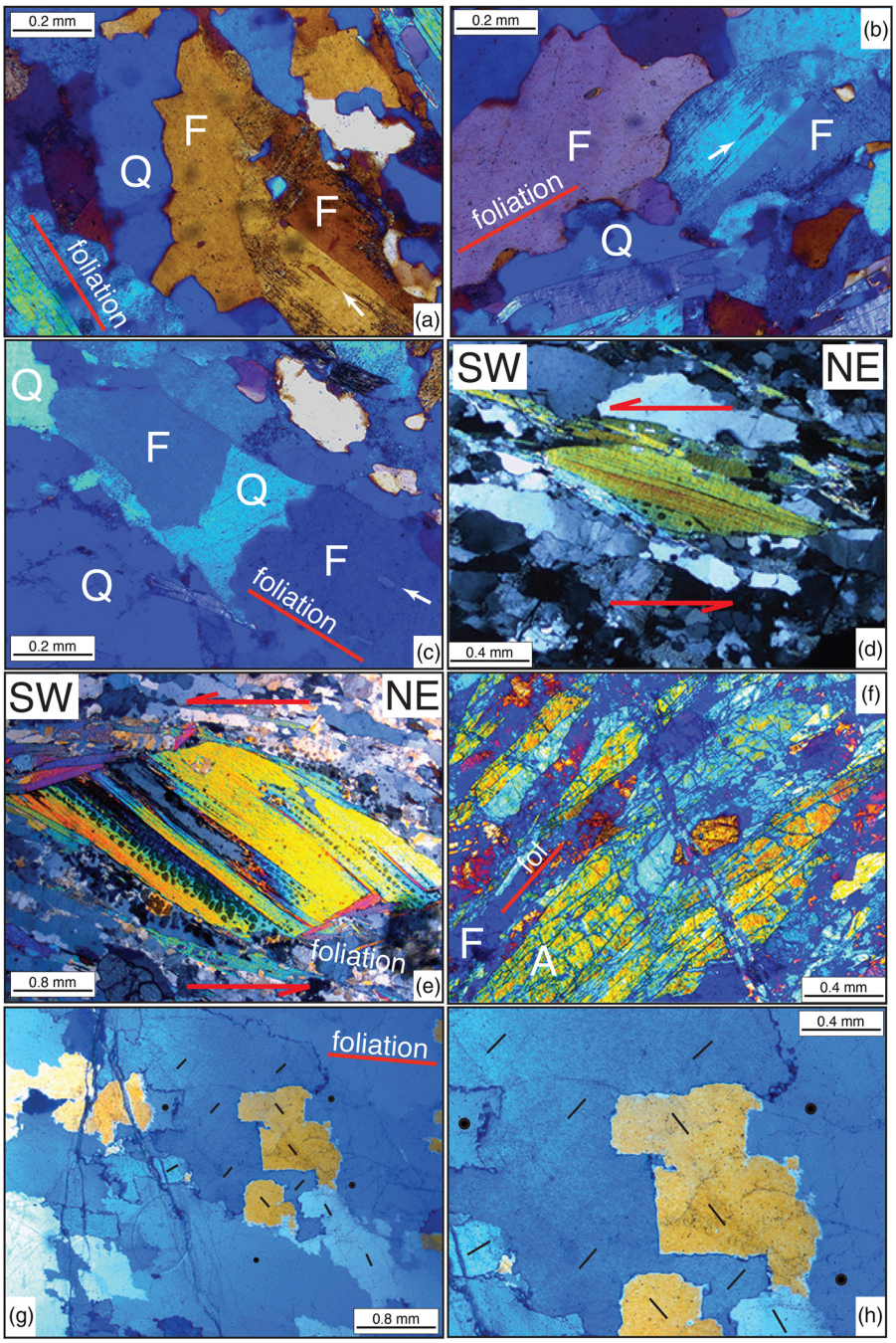

Fig. 8. Photomicrographs of gneisses and a sheared quartz vein from the NE section of Rosemarkie Inlier; all micrographs are viewed geographically downwards onto sections cut perpendicular to the foliation and parallel to NE-plunging lineation; all micrographs are in cross-polarized light and, with the exception of (d), were taken with a mica plate inserted and are shown with false colours to emphasize the microstructures; the orientation of the macroscopic foliation for individual micrographs is indicated; the map positions are indicated in Figure 4. (**a**)–(**e**) Gneiss sample RM-22-07; lobate boundaries between quartz (Q) and feldspar (F) grains; note (a) and (b) the wedge-shaped deformation twins (arrowed) in the feldspar grain, and (c) the foliation-parallel inclusions (arrowed) in the feldspar grain; (d) and (e) mica fish indicate a sinistral shear sense. (**f**) Amphibolite sample RM-22-09; amphibole laths (A: light blue–yellow–red in the false colour image) orientated parallel to the macroscopic foliation and cut by numerous fractures at a high angle to the foliation (and lineation). (**g**) and (**h**) Sheared quartz vein sample RM-23-01; note two sets of straight and mutually perpendicular boundaries of a quartz grain in the centre of the micrographs, with smaller lobes on the grain boundaries; the boundaries of the grain are sub-parallel (5° counterclockwise) and sub-perpendicular to the macroscopic trace of the foliation on the *XZ* plane; the local trend of *c*-axes on the *XZ* plane within individual grains is indicated by black bars, and *c*-axes sub-perpendicular to the *XZ* plane are indicated by black circles; top left to bottom right- and top right to bottom left-trending *c*-axes correspond to the leading and trailing edges of associated quartz *c*-axis fabrics (see next section on Quartz *c*-axis fabrics).

(Fig. 4). A solid-state foliation within the granite (Fig. 6c–f) is parallel to the margins of the sheet and overprints any original magmatic or submagmatic flow fabric that may have developed. This granite sheet was originally described by Stewart (2010, location 14.7B) and is located *c*. 1.25 km to the NE of the similarly orientated granite sheets used by Mendum and Noble (2010) for isotopic dating (see above). The granite sheet strikes parallel to foliation in the surrounding gneisses. A grain-shape lineation on the foliation surface of sample RM-22-03 plunges at 16° towards 078° (Fig. 6d), sub-parallel to the lineation in the adjacent gneisses and amphibolites. Stewart (2010, fig. 14.5d) described asymmetrical orthoclase feldspar porphyroclasts and shear bands from the granite sheet that indicate a sinistral shear sense viewed vertically downwards on a geographically horizontal wave-polished erosion surface. Preparation of orientated and polished slabs from sample RM-22-03 has confirmed the observations and sinistral shear-sense interpretation of Stewart (2010), and in particular has revealed the presence of shear bands and asymmetrical feldspar porphyroclasts with sigma-shaped wings composed of ribbons of comminuted (minutely fractured) white-pink feldspar and white-glassy plastically deformed quartz (Fig. 6e, f). In thin section, foliation in the penetratively sheared/mylonitic granites is typically defined by ribbon-like domains of recrystallized quartz interlayered with much larger equant to elongate single and polycrystalline grains of feldspar orientated at varying angles to ribbon-defining foliation (Fig. 9a, b). While some microcracks cut across both the quartz and feldspar grains, many are confined to individual feldspar grains (Fig. 9b). A deformation temperature of *c.* 450°C is inferred from these microstructures (plastic deformation of quartz, but brittle deformation of feldspar).

Quartz *c*-axis fabrics

From the samples collected from the NE section of the Rosemarkie Inlier, only three contained sufficient quartz for fabric analyses. These included gneiss samples RM-22-07 and RM-22-05 and sheared quartz vein sample RM-23-01 (Fig. 4). All three samples are characterized by cross-girdle fabrics intersecting the foliation at right angles to the lineation (Fig. 10a, b). By analogy with

experimental and numerical modelling studies (e.g. Lister 1977; Tullis 1977; Lister *et al.* 1978; Lister and Hobbs 1980; Heilbronner and Tullis 2006), the cross-girdle fabrics indicate deformation under close to plane-strain conditions with the mineral lineation orientated parallel to the maximum principal stretch direction in all three samples examined.

Gneiss sample RM-22-07 was collected at the northern end of the NE section, 150 m to the SE of granite sheet RM-22-03 (Fig. 4). Sample RM-22-07 yielded an asymmetrical Type II (Lister 1977) cross-girdle fabric (Fig. 10a) formed by two planar (great circle) distributions of *c*-axes crossing each other close to the sample *Y* direction. Measured in the *XZ* plane, the C1 (36°) and C2 (45°) angles between the foliation pole and the leading and trailing edges of the cross-girdle fabric indicate a sinistral shear sense (Fig. 10c) that is confirmed by the sense of inclination of the central section of the cross-girdle fabric to the foliation (Fig. 10d). As noted above, this shear sense was also indicated by asymmetrical white mica fish in sample RM-22-07 (Fig. 8d, e). This sinistral shear sense is consistent with a NW side up to the SW and SE side down to the NE sense of motion parallel to the moderately ENE-plunging lineation (Fig. 11b, c). The opening angle (81°) in sample RM-22-07 (Fig. 11a) indicates a deformation temperature of *c.* 610°C using the linear opening angle thermometer of Faleiros *et al.* (2016). This estimated deformation temperature is compatible with, but at the low temperature end of, the range of deformation temperatures indicated by both feldspar and quartz GBM microstructures in this sample (see above).

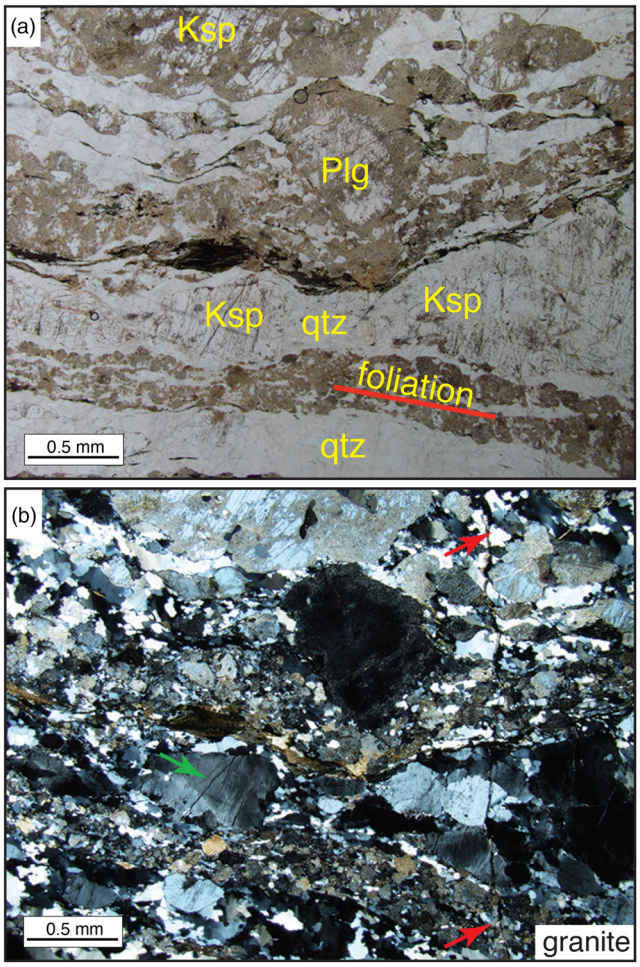

Fig. 9. Photomicrograph pair taken in (**a**) plane-polarized light and (**b**) cross-polarized light illustrating typical grain-shape foliation in the sheared/mylonitic granites (the location shown in Fig. 3b) defined by elongate to ribbon-like domains of recrystallized quartz interlayered with much larger equant to elongate feldspar grains in varying orientations. Note the cracks orientated at a high angle to the foliation; a large crack (red arrows) cuts across both quartz and feldspar grains, while smaller and more numerous cracks (e.g. at the green arrow) are confined to individual feldspar grains. Ksp, orthoclase feldspar; Plag, plagioclase feldspar; qtz, quartz.

Gneiss sample RM-22-05 was collected 1250 m to the SSE of sample RM-22-07 (Fig. 4) in the part of the coastal section where granite intrusions (isotopically dated by Mendum and Noble 2010) are most abundant and particularly well exposed. Sample RM-22-05 yielded a transitional Type I to Type II (Lister 1977) cross-girdle fabric (Fig. 10a) in which an approximate small circle distribution of *c*-axes about the foliation pole (*Z*) is connected by a partial great circle of *c*-axes passing through the sample *Y* direction at right angles to lineation (*X*). Both the C1 and C2 angles between the foliation pole and the cross-girdle fabric (Fig. 10c) and the inclination of the central section of the cross-girdle fabric to the foliation (Fig. 10d) indicate a sinistral shear sense, with the leading edge of the cross-girdle fabric making a C1 angle of 31° with the foliation pole, while the trailing edge makes an angle of 36°. As in sample RM-22-07, the sinistral shear sense indicated by the asymmetrical *c*-axis fabric is consistent with a NW side up to the SW and a SE side down to the NE sense of motion associated with the moderately NE-plunging mineral lineation. The opening angle (C1 + C2 = 67°) of the cross-girdle *c*-axis fabric from sample SG-22-05 was significantly smaller than in sample RM-22-7, indicating a deformation temperature of *c.* 510°C using the linear opening angle thermometer of Faleiros *et al.* (2016). The inferred deformation temperature was significantly lower than the likely deformation temperature range (>675°C) indicated by the accompanying feldspar GMB microstructures in sample RM-22-05, probably indicating that the quartz *c*-axis fabric continued to evolve during cooling/exhumation, with the now preserved quartz fabric reflecting only the later and cooler stages of deformation. This interpretation is consistent with the GBB microstructures observed at the margins of some feldspar and quartz grains that indicate temperatures of less than *c.* 450–500°C (see above). However pervasive shearing is unlikely to have continued significantly below *c.* 500°C as the feldspar grains remain unfractured and there is no microstructural evidence for subgrain rotation recrystallization (SGR) of quartz, which occurs in the *c.* 400–500°C temperature range (see the review by Law 2014).

Sheared quartz vein sample RM-23-01 was collected (Fig. 4) from the side of a 30 cm-wide granite sheet located 50 m to the SE of gneiss sample RM-22-05 and *c.* 25 m to the SE of one of the granite intrusions isotopically dated by Mendum and Noble (2010, sample GX.1734). Sample RM-23-01 yielded a strongly defined Type I cross-girdle fabric (Fig. 10a) that passes through the sample *Y* direction at right angles to the lineation (*X*). A straight leading edge in the fabric is particularly well defined in this sheared quartz vein, and its inclination (ψ) to foliation indicates a sinistral shear sense (Fig. 10d), once again consistent with a NW side up to the SW and a SE side down to the NE sense of motion associated with the steeply NE-plunging mineral lineation. The leading fabric edge makes a C1 angle of 36° to the foliation pole measured in the *XZ* plane. However, the trailing fabric edge is not populated with *c*-axes close to the *XZ* plane and the C2 angle is difficult to define, with possible C2 angles projected from the parts of the trailing edge closer to the sample *Y* direction ranging from *c.* 29° to 46° (Fig. 10c, d). The possible combined C1 + C2 opening angle is therefore in the range 65°–82°, with associated deformation temperatures of 495–615°C using the linear opening angle thermometer of Faleiros *et al.* (2016). Blocky or chessboard extinction was observed in some of the quartz grains, suggesting at least a component of high-temperature (>630°C) prism <*c*> slip. Straight rectilinear boundaries intersecting at right angles were observed around large (250–1000 μm) square to rectangular quartz grains (Fig. 8g, h) with

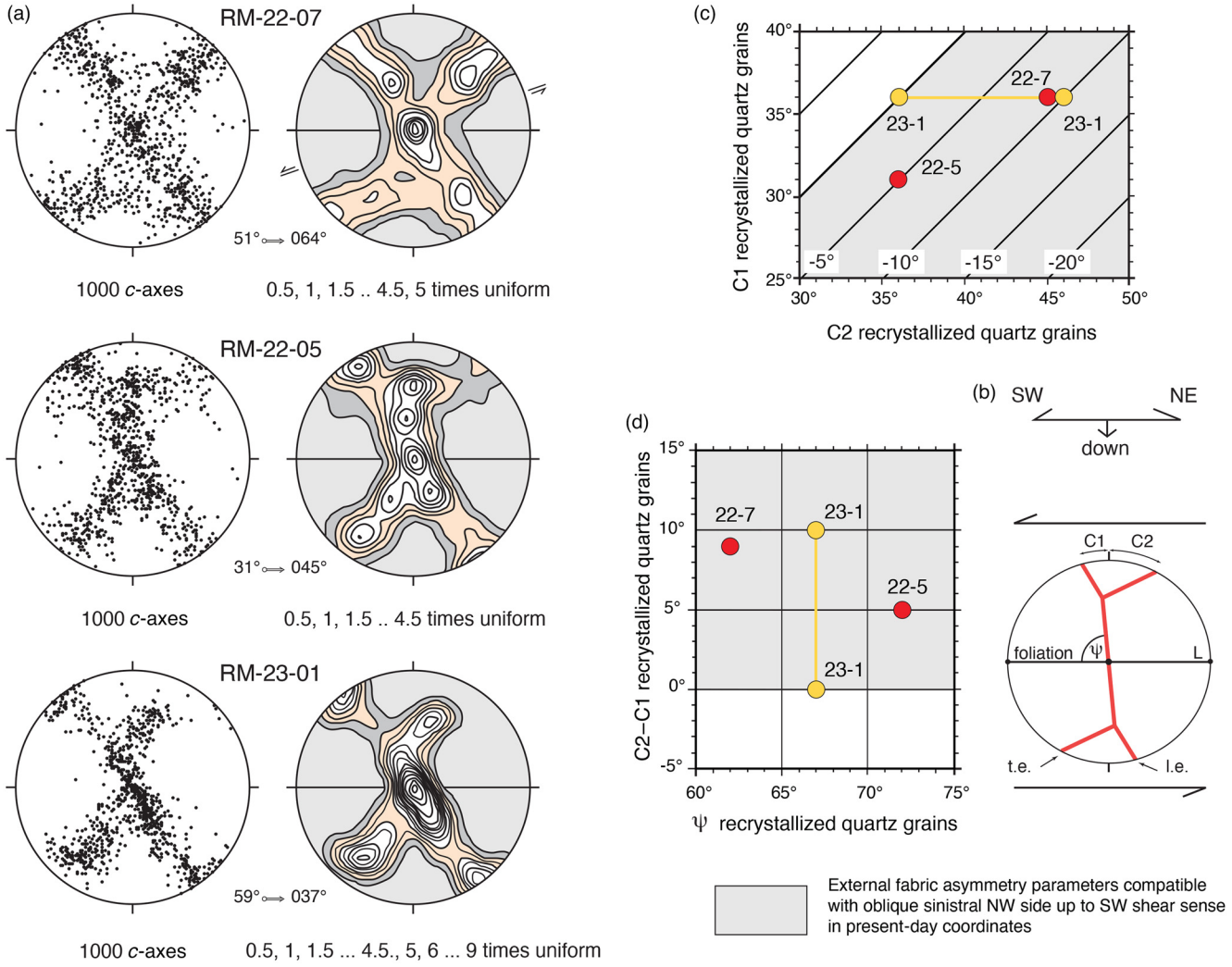

Fig. 10. Quartz *c*-axis fabric data for gneiss samples RM-22-07 and RM-22-05 and sheared quartz vein RM-23-01. (**a**) Quartz fabric data are displayed on lower-hemisphere, equal-area projections orientated perpendicular to the foliation and parallel to the mineral lineation; the plunge and trend of the lineation are indicated; the orientation of the shear bands in RM-22-07 is indicated. (**b**) Explanation of the external fabric asymmetry components. te, trailing edge of the fabric skeleton; le, leading edge of the fabric skeleton. (**c**) Relationships between the C1 and C2 external asymmetry parameters for the three samples analysed; note the 10° uncertainty in determining the C2 angle for sample RM-23-01. (**d**) Relationships between C2–C1 and ψ external asymmetry parameters for the three samples analysed. Note the 10° uncertainty in determining the C2–C1 angle for sample RM-23-01.

internal blocky extinction. Similar microstructures have been recorded in high-grade (amphibolite- to granulite-facies) metamorphic rocks (Lister and Dornsiepen 1982; Lister and Snoke 1984), and are thought to have been caused by the interaction of migration recrystallization with grain-boundary sliding. An order of magnitude smaller (20–50 μm) bulges on these grain boundaries (similar to the bulges seen in gneiss samples RM-22-07 and RM-22-05, see above) are interpreted to indicate late low-temperature (300–400°C) GBB recrystallization of quartz.

As suggested in the previous section based on quartz and feldspar microstructures, the quartz *c*-axis fabrics in our three samples appear to have been 'frozen in' at somewhat different deformation temperatures during progressive shearing, cooling and exhumation of the Rosemarkie rocks.

Monazite–xenotime petrochronology in the NE section of the Rosemarkie Inlier

Within our samples from the Rosemarkie Inlier, monazite and xenotime grains were only found in gneiss sample RM-22-08, which was collected from the same outcrop as (and within 10 cm of) sample RM-22-07 (Figs 4 and 6a), which, as discussed above, yielded an asymmetrical cross-girdle quartz *c*-axis fabric indicating an oblique sinistral (NW side up to the SW) shear sense and a deformation temperature of *c.* 610°C. Petrochronological analysis of these phases was undertaken to: (1) document the crystallization history of these grains and their potential for constraining the timing of the structural/kinematic evolution of the rocks as indicated by microstructures and crystal fabrics; (2) calculate the crystallization temperatures indicated by monazite–xenotime thermometry and compare these temperatures with deformation temperatures indicated by microstructures and crystal fabric; and (3) compare the monazite and xenotime crystallization histories from the gneisses with the monazite and zircon crystallization ages of the granite sheets documented by Mendum and Noble (2010), and use the combined datasets to refine the exhumation history for the Rosemarkie Inlier. We also compare the Rosemarkie monazite and xenotime crystallization ages with similar datasets in the NHT, and compare the exhumation history deduced from the Rosemarkie Inlier with recently published exhumation histories for the NHT.

Results of monazite–xenotime petrochronology

A total of 14 monazite and three xenotime grains in sample RM-22-08 were analysed *in situ* by LASS to determine the U–Pb ages and

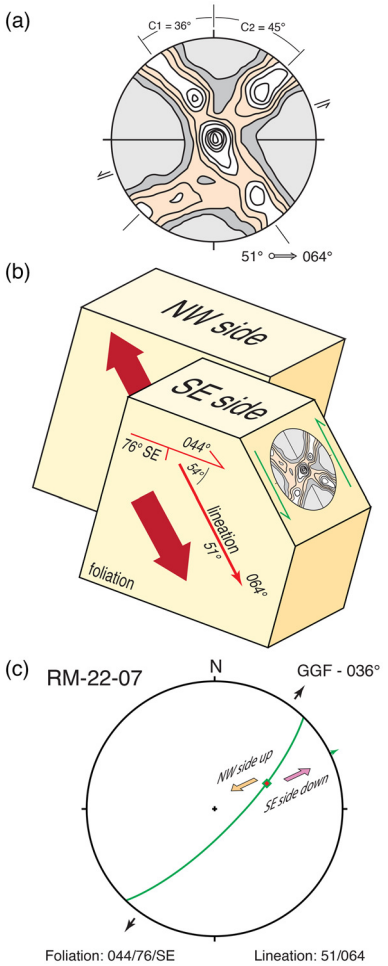

Fig. 11. Explanation of the 3D shear sense determined for gneiss sample RM-22-07. (**a**) The quartz *c*-axis fabric diagram is orientated perpendicular to the foliation, parallel to the mineral lineation and is viewed geographically downwards. The orientations of the shear bands and the C1 and C2 angles between the pole to foliation and the leading (C1) and trailing (C2) edges of the fabric skeleton are indicated. (**b**) A block diagram illustrating oblique sinistral shearing inferred from the shear bands and fabric asymmetry. (**c**) Lower-hemisphere, equal-angle plot summarizing the oblique sinistral shearing; the foliation represented by green great circle; the mineral lineation is indicated by the diamond symbol; the local strike of the Great Glen Fault Zone (GGFZ) is indicated by arrows. Source: (**c**) the strike of the GGFZ is from Highton (2009) and Mendum and Noble (2010).

trace element compositions. WDS X-ray images were subsequently collected by electron microprobe for all of the analysed grains. The compositional zoning of Y, Th, Si and Ca in the monazite was distinctive and complex, with clear core and rim textures present in most grains (Fig. 12a, b; see also Supplementary Table 1). However, a straightforward growth sequence of evolving monazite composition is difficult to discern from our imaging. For example, the monazite grains in sample RM-22-08 do not have consistently low Y core domains and high Y rims. Rather, some grains have low Y core domains (mon16 in Fig. 12), while others have high Y core domains (mon6 in Fig. 12), and yet others have minimal Y zoning but distinctive core–rim domains defined by Th and Si zoning (mon9 in Fig. 12). There are two potential explanations for these observations. First, the REE and phosphate contents may be heterogeneously distributed in the rock, resulting in local reactions controlling the evolving monazite composition during growth. Alternatively, it is possible that a consistent sequence of evolving compositional domains did grow throughout the sample, but an inconsistent set of growth domains is preserved in each grain. While it is difficult to distinguish between these potential explanations given the present data, U–Pb analyses do provide some insight (see below).

We have used compositional domains on a grain-by-grain basis to distinguish core and rim analyses, rather than attempting to correlate domains of specific compositions across grains. Fifteen analyses were placed in core domains, five of which were rejected due to greater than 10% discordance. 2σ absolute uncertainties are reported for each age and propagated additional 1% external uncertainties are given in parentheses. The calculated concordia age for the accepted monazite core analyses was 418.9 ± 3.0 (5.2) Ma and a weighted average of the $^{206}Pb/^{238}U$ ages was 418.2 ± 3.3 (5.3) Ma (Fig. 13a). Forty-six analyses were placed in rim domains, 23 of which were rejected due to greater than 10% discordance. The calculated concordia age for the accepted monazite rim analyses was 403.0 ± 1.9 (4.5) Ma and a weighted average of the $^{206}Pb/^{238}U$ ages was 401.8 ± 2.7 (4.8) Ma (Fig. 13b). The calculated concordia age for the xenotime analyses was 405.5 ± 2.8 (4.9) Ma and a weighted average of the $^{206}Pb/^{238}U$ ages was 404.5 ± 4.6 (6.1) Ma, with two of the 12 analyses rejected (Fig. 13c). Returning to an earlier question, if a consistent set of compositional domains across the sample were inconsistently preserved in individual monazite grains, we would expect more overlap in the ages of apparent rim and core domains. For example, a high Y domain might be a core in one grain and a rim in another grain. As our core and rim analyses are fairly well-defined statistical populations, it seems more likely that the differing apparent imaged compositions of cores and rims between grains reflect local controls on the composition of monazite growing at particular times (e.g. Williams *et al.* 2007, 2017). However, the uncertainties in individual analyses are large enough that it is difficult to be confident about this conclusion.

Trace element compositions were used for monazite–xenotime thermometry based on the methods outlined in Mako *et al.* (2024). Trace element compositions measured by LASS were very similar across all domains (Fig. 13d), despite the distinct zoning apparent in the WDS images (Fig. 12). The only distinguishing compositional feature of the core domains is the less pronounced Eu anomalies for most analyses, while some apparent core analyses have Eu anomalies that are indistinguishable from the rim domains (Fig. 12). Monazite rims and xenotime have ages that overlap within uncertainty, which is permissive of the equilibrium between these phases. The calculated X_{Y+HREE} compositions of the rim domains (where X refers to the mole fraction of Y + HREE in monazite (X_{Y+HREE})) constitute a nearly normal distribution, with an average of about $X_{Y+HREE} = 0.073$ (Fig. 14a). This results in a temperature of 616 ± 25°C based on the Pyle *et al.* (2001) calibration of data analysed by Heinrich *et al.* (1997). Monazite core domain analyses exhibit a wider range of compositions, with a probability peak at $X_{Y+HREE} = 0.083$, which results in a temperature of *c.* 650°C (Fig. 14b). Xenotime that overlaps in age with monazite core domains was not observed in this study, so this constitutes a minimum temperature. A robust temperature–time point on the metamorphic path for the Rosemarkie Inlier can thus be established at 401.8 ± 4.8 Ma at 616 ± 25°C from monazite rims. In addition, monazite cores recorded temperatures greater than *c.* 650°C at 418 ± 5 Ma.

The crystallization temperature of 616 ± 25°C for monazite rims indicated by the monazite–xenotime thermometry for gneiss sample RM-22-08 is remarkably similar to the deformation temperature of 610°C indicated by the quartz *c*-axis fabric opening angle in sample RM-22-07 using the linear opening angle thermometer of Faleiros *et al.* (2016) and collected from the same outcrop (see above). In summary, we interpret this close correspondence in temperature estimates as indicating that the monazite rims grew at mid-crustal levels during oblique sinistral shearing recorded by the mylonitic quartz fabrics at *c.* 402 Ma.

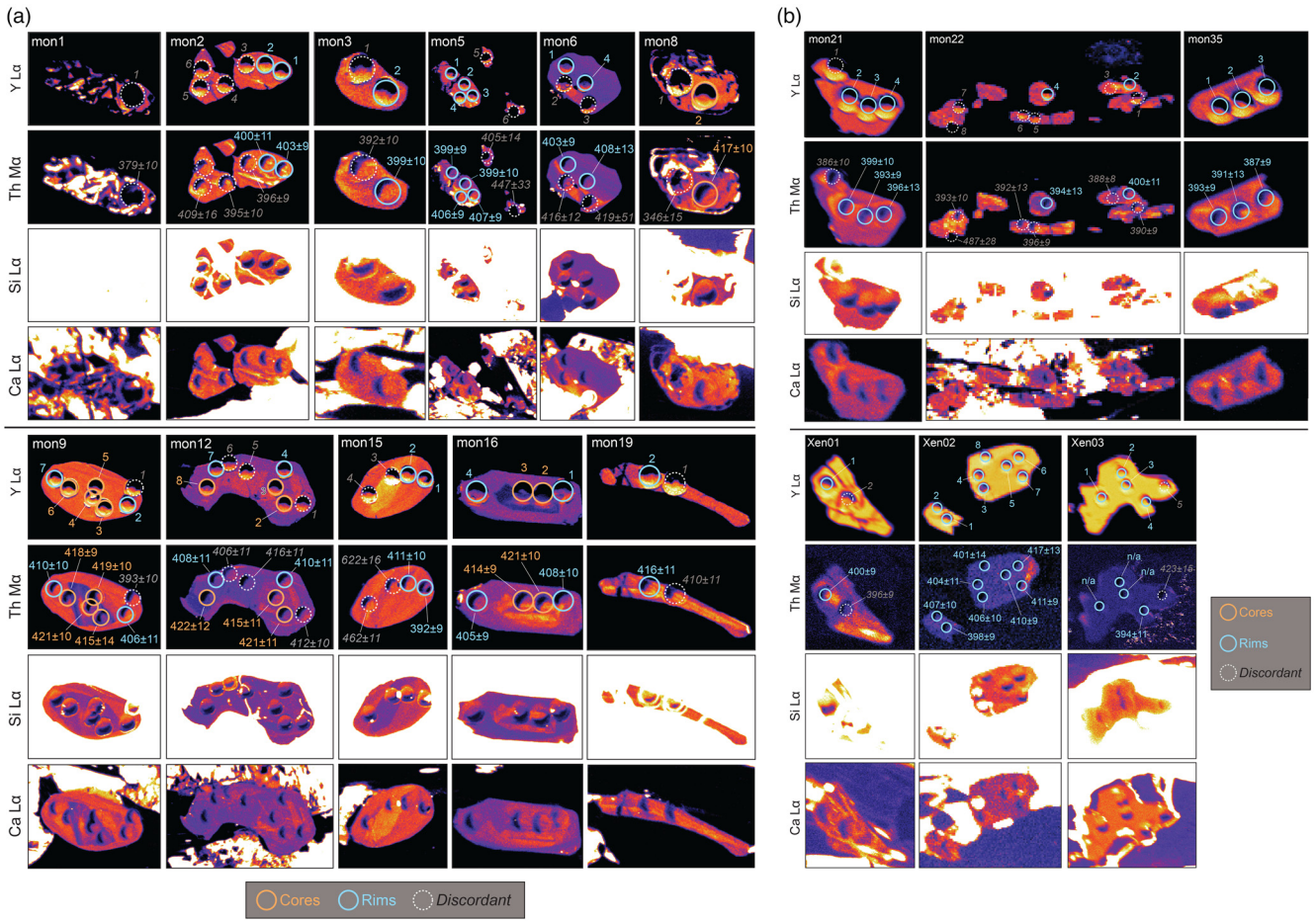

Fig. 12. (**a**) and (**b**) Electron microprobe wavelength-dispersive spectrometry (WDS) images of select elements for monazite (mon) and xenotime (Xen) grains from sample RM-22-08. Laser ablation spots are coloured according to the textural domain (core, orange circles; rim, blue circles) and discordance (dashed circles). $^{206}Pb/^{238}U$ ages (Ma), with 2σ internal uncertainties, for each spot are given in the top row. All monazite images were simultaneously processed, with X-ray counts standardized to the same colour across all grains for a given element. Warmer colours (yellow–white) indicate higher X-ray counts and cooler colours (purple–black) indicate lower X-ray counts.

Comparison of monazite–xenotime thermometry and age data from the Rosemarkie Inlier and the Northern Highland Terrane

Geochronological data from the present study contrasts with published data from the NHT (Fig. 15). The northernmost part of the NHT preserves a series of WNW-directed ductile thrust nappes developed structurally above the brittle–ductile Moine Thrust Zone (e.g. Strachan *et al.* 2002, 2020; Thigpen *et al.* 2013; Ashley *et al.* 2015; Law *et al.* 2024). Peak temperatures in the hinterland Naver Nappe were as high as 700°C at *c*. 425 Ma, followed by 5–10 Myr of slow cooling (Mako *et al.* 2019). Monazite–xenotime thermometry in combination with $^{40}Ar/^{39}Ar$ muscovite geochronology from the structurally lower Moine and Ben Hope nappes then records a period of very rapid cooling at 415–410 Ma, and final exhumation by 407–403 Ma (Spencer *et al.* 2020, 2021; Mako *et al.* 2024). In addition, monazite–xenotime thermometry from an isolated exposure of Moine rocks on the Creich Peninsula (Fig. 15) recorded temperatures of 610°C at 422 ± 2 Ma (Mazza *et al.* 2018; Mako 2019).

The Rosemarkie Inlier monazite cores that record temperatures greater than 650°C at 419 ± 5 Ma are broadly consistent with the thermal structure of the Scandian hinterland recorded in the NHT thrust nappes (e.g. Thigpen *et al.* 2013; Mako *et al.* 2019). However, our monazite rim data (616 ± 25°C at 401.8 ± 4.8 Ma) suggest that high-temperature deformation and metamorphism in the inlier far outlasted the high-temperature thermal structure recorded in the thrust nappes located *c.* 70–120 km to the NW of the offshore position of the GGFZ (Fig. 15). This in turn suggests that mid-crustal oblique sinistral shearing and mylonitization at mid-crustal levels on the GGFZ occurred some 10–15 Myr after regional thrust-related shearing and metamorphism at similar crustal levels had ceased in the NHT, and was succeeded by uplift, cooling and exhumation by Lower Devonian (Emsian, 407–393 Ma) times. An implication of our findings is that the Rosemarkie Inlier exposes GGFZ-related mylonites that must be bounded to the NW by a tectonic boundary that is now obscured by unconformably overlying Devonian sedimentary rocks (Fig. 2) and/or later brittle faults.

Exhumation history of the Rosemarkie Inlier

Our combined microstructural, crystal fabric, isotopic dating and monazite–xenotime thermometry indicates that the gneisses in at least the NE section of the Rosemarkie Inlier were deforming at temperatures of *c*. 615°C at 401.8 ± 4.8 Ma. As outlined above, these basement gneisses are unconformably overlain by Middle Devonian conglomerates and sandstones. Fletcher *et al.* (1996, table 1) listed these sedimentary units as Eifelian in age (393.3 ± 1.2–387.7 ± 0.8 Ma; stratigraphic age range after Cohen *et al.* 2013, updated 2023). Fossil spores from this sequence (Richardson 1960), supported by correlation with the Achanarras Fish Bed of the Orcadian Basin, indicate that the basal beds were deposited in either the middle (Rogers *et al.* 1989, fig. 2 – Cromarty & Nig column) or late Eifelian (Marshall *et al.* 2007; Marshall 2024, fig. 9.4).

Taking a 402 Ma age for the shearing at 615°C and a mid-Eifelian age of 390 Ma for exhumation to the Devonian land surface

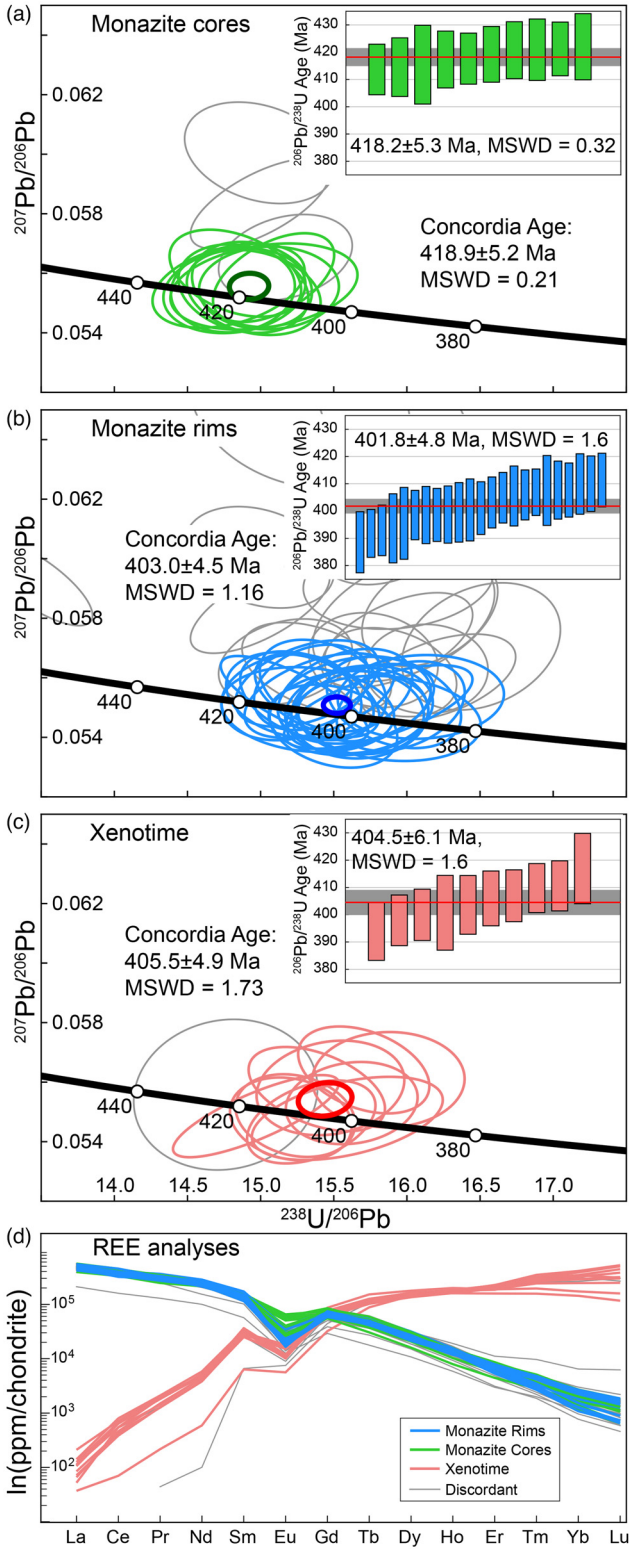

Fig. 13. Tera–Wasserburg diagrams of U–Pb data and trace element data from sample RM-22-08. All data are plotted with 2σ internal uncertainties. The inset bar graphs show weighted averages of $^{206}Pb/^{238}U$ ages for concordant analyses. (**a**) U–Pb data and concordia age for monazite cores. (**b**) U–Pb data and concordia age for monazite rims. (**c**) U–Pb data and concordia age for xenotime. (**d**) Chondrite-normalized REE data for all analysed monazite and xenotime, colour-coded by domain.

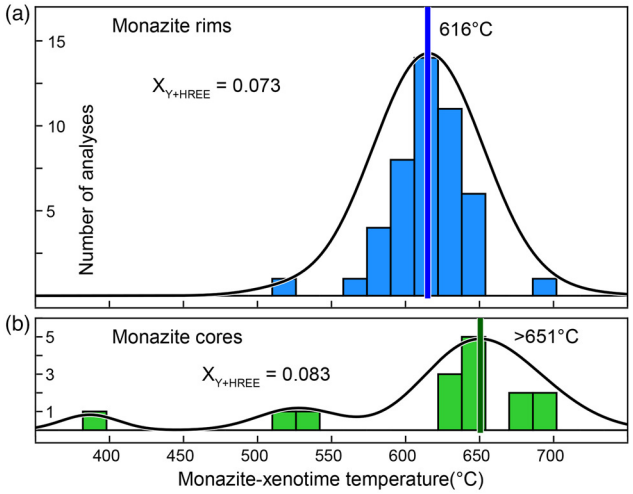

Fig. 14. Histograms and relative probability plots for monazite rim and core compositions. The temperature from the monazite–xenotime thermometry was calculated for each laser ablation analysis using the Pyle *et al.* (2001) calibration equation based on the data of Heinrich *et al.* (1997). (**a**) Monazite–xenotime thermometry for rim domain analyses yields a temperature of 616 ± 25°C. (**b**) Monazite–xenotime thermometry for core domain analyses yields a temperature of about 651°C. Because none of the dated xenotime overlaps in age with the monazite cores, this should be regarded as a minimum temperature.

(Fig. 16; see the red and white circles in boxes with lengths denoting the uncertainty in the age of the monazite rims and the age range of the Eifelian) indicates a time-averaged cooling rate of *c.* 50°C Ma^{-1}. In contrast, a faster time-averaged cooling rate of *c.* 150°C Ma^{-1} would be indicated by taking a *c.* 397 Ma age for the shearing at 615°C and exhumation to the land surface at *c.* 393 Ma, while a slower time-averaged cooling rate of *c.* 30°C Ma^{-1} would be indicated taking a *c.* 407 Ma age for the shearing at 615°C and exhumation to the land surface at *c.* 387 Ma.

To date, there are no quantitative barometric data to directly estimate the crustal depth at which shearing at 615°C occurred. Assuming a geothermal gradient of 30°C km^{-1} (and that negligible shear heating or heating associated with the intrusion of felsic/granitic magma occurred in the fault zone) yields a calculated depth of *c.* 21 km for the shearing at 615°C (Fig. 16) and a time-averaged exhumation rate of *c.* 1.75 km Ma^{-1} (1.75 mm a^{-1}) to the Devonian land surface at 390 Ma. Time-averaged exhumation rates of 1.47, 2.10 and 2.60 km Ma^{-1} would be indicated for assumed geothermal gradients of 35, 25 and 20°C km^{-1}, respectively. These estimated exhumation rates fall within the broad spectrum of steady-state erosion rates estimated for different orogenic settings, ranging from as low as *c.* 0.3–0.75 km Ma^{-1} in the Olympic Mountains and European Alps to as high as 3–5 km Ma^{-1} in the Himalaya and Taiwan (see Spencer *et al.* 2020 for a review and discussion). The near-equatorial (*c.* 15° S) latitude of Scotland in the late Silurian–early Devonian (Cocks and Torsvik 2011) indicates a temperate to subtropical climate, with fluvial and hillslope diffusion processes being the dominant erosion mechanisms.

Mendum and Noble (2010) proposed that the Rosemarkie Inlier was tectonically exhumed as an elongate 'pip' at a sharp restraining bend on the Great Glen Fault during sinistral transpression. They suggested that exhumation was associated with constrictional strains and tracked the moderately NE-plunging stretching lineation that structurally dominates the NE coastal section of the Rosemarkie Inlier. However, given the change from NE- to SW-plunging lineation traced from the NE section to the Central section of the inlier (Figs 3b–5) and the quartz fabrics (Fig. 10a) that indicate penetrative deformation occurred under plane strain rather than constriction, it seems unlikely that the basement rocks would have followed such a simple inclined (NE-plunging) and tectonically driven exhumation path.

Exhumation rate data from restraining bends on current or recently active steeply dipping strike-slip fault zones appear to be very limited compared with erosion rate data from mountain belts.

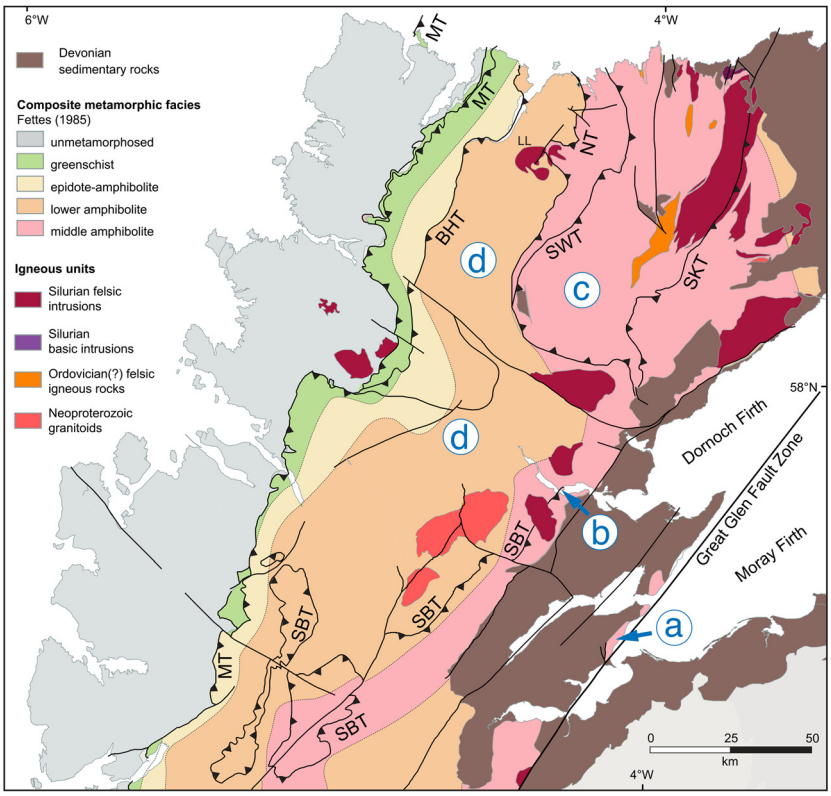

Rosemarkie Inlier: oblique sinistral strike slip with NW side up to SW. Sinistrally sheared leucogranites: 397.6 ± 2.2 Ma monazite age (Mendum & Noble 2010). Sinistrally sheared gneissic psammites: monazite rims: 401.8 ± 4.8 Ma; monazite cores: 418.2 ± 5.3 Ma; xenotime: 404.5 ± 6.1 Ma (this study). Unconformably overlain by Eifelian (393-387 Ma) sedimentary rocks.

Sgurr Beag thrust on Creich Peninsula: top down to ESE normal sense motion. Scandian monazite population at 420 ± 5.0 Ma with separate Precambrian population (Mazza *et al.* 2018, Mako 2019).

Naver / Skinsdale thrust sheets: Top to NW thrusting. Monazites range from 428.7 ± 4.9 Ma to 416.7 ± 4.6 Ma (Mako *et al.* 2019). Unconformably overlain by Emsian (407-393 Ma) sedimentary rocks.

Moine and Ben Hope thrust sheets: Top to NW thrusting. Monazites range from 416.0 ± 5.0 Ma to 412.0 ± 4.0 Ma (Mako *et al.* 2024). Unconformably overlain by Emsian (407-393 Ma) sedimentary rocks.

Fig. 15. Summary of the monazite–xenotime age data for the Rosemarkie Inlier and adjacent parts of the Northern Highland Terrane (NHT). Note that the oldest monazite ages are recorded in the middle amphibolite-facies Naver/Swordly thrust sheet. Monazite rims from sheared gneisses exposed in the Rosemarkie Inlier yield the youngest monazite ages recorded in the NHT. Previously published ages and uncertainties for the NHT have been recalculated using the same uncertainty procedure as adopted for the Rosemarkie Inlier. MT, Moine thrust; BHT, Ben Hope Thrust; NT, Naver Thrust, SWT, Swordly Thrust; SKT, Skinsdale Thrust; SBT, Sgurr Beag Thrust. Source: the metamorphic facies are modified from Fettes *et al.* (1985).

Lease *et al.* (2021), using apatite (U–Th)/He data, estimated exhumation rates since 0.4 Ma of 5–10 mm a^{-1} (5–10 km Ma^{-1}) localized on a restraining bend on the currently active Fairweather Fault in Alaska, which is reputed to be the Earth's fastest-slipping intracontinental strike-slip fault. Similarly, Spotila *et al.* (2001), also using apatite (U–Th)/He data, estimated exhumation rates of *c.* 5–7 mm a^{-1} on strands of the San Andreas Fault System in southern California that were sustained for at least several hundred thousand years, with erosion probably keeping pace with rock uplift to maintain a steady-state topographical relief. These examples are at the fast end of a likely spectrum of exhumation rates on current or recently active strike-slip fault zones. Towards the slower end of the spectrum, Baden *et al.* (2024), using apatite (U–Th)/He and other previously published thermochronology datasets, estimated a maximum exhumation of *c.* 2.5 km since *c.* 4 Ma on the Santa Cruz Mountain section of the San Andreas Fault System in central California, which equates to a time-averaged exhumation rate of 0.625 mm a^{-1}. Similarly, using apatite (U–Th)/He and other thermochronology datasets, Cochran *et al.* (2017) documented exhumation rates since the late Miocene (6 Ma) of 0.8–2.0 mm a^{-1} on a restraining bend in the Enriquillo–Plantain Garden Fault in Jamaica. This currently active strike-slip fault system may be a particularly appropriate analogue for the GGFZ given its tropical setting in late Silurian–Lower Devonian times. We should note here, however, that although our time-averaged exhumation rate for the Rosemarkie Inlier falls within the range of exhumation rates on these current/recently activate strike-slip fault systems, we are not aware of any current/recently active strike-slip fault systems on which 12 ± 8 Ma amphibolite-facies mid-crustal rocks have been exhumed.

Our estimated exhumation rate of *c.* 1.75 mm a^{-1} for the Rosemarkie Inlier, which is time-averaged over a longer time period (*c.* 12 Myr) than the above studies, is broadly compatible with exhumation rates at the slower end of the spectrum of rates (0.625–2.0 mm a^{-1}) for currently/recently active strike-slip fault systems. As noted above, our estimated exhumation rate also falls within the range of erosion rates (*c.* 0.5–5 mm a^{-1}) estimated for currently active mountain ranges. Therefore, our exhumation rate data cannot by itself distinguish between the likely influence of erosion and tectonically driven exhumation on the unroofing of the Rosemarkie Inlier in Lower Devonian times. However, as noted above, the monazite rim crystallization ages of 402 Ma in the Rosemarkie Inlier are the youngest monazite ages recorded in the NHT (Fig. 15). We suggest that the localization of these young monazite crystallization ages on the SE margin of the NHT and adjacent to the GGFZ would argue for focused fault-driven early Devonian (Emsian–Eifelian: Fig. 16) exhumation of fault-related sinistral mylonites from mid-crustal depths, consistent with exhumation driven by strike-slip tectonic processes, as broadly envisaged by Mendum and Noble (2010).

On the NW side of the fault zone, rocks assigned to the NHT are affected by Scandian (Silurian) metamorphism (Fig. 15) and are locally unconformably overlain by Emsian (407.6 ± 2.6–393.3 ± 1.2 Ma: Cohen *et al.* 2013, updated 2023) fluvial sedimentary rocks

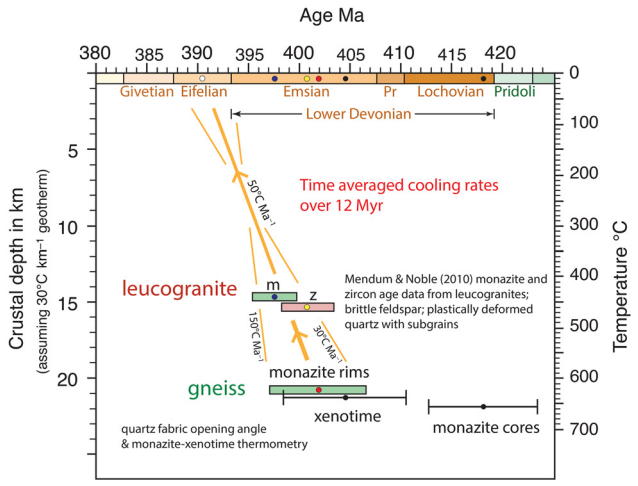

Fig. 16. Summary of temperature and isotopic age data for gneissic psammites and granites from the Rosemarkie Inlier. Gneisses: sample RM-22-07 – deformation temperature of 610°C indicated by the quartz *c*-axis fabric opening angle; gneiss sample RM-22-08 – crystallization temperature of 615°C indicated by monazite–xenotime thermometry. Granites: deformation temperature of *c*. 450°C indicated by the plastic deformation of quartz and the brittle deformation of feldspar clasts in sample RM-22-03 and leucogranite intrusions described by Mendum and Noble (2010). Age ranges (2σ) shown for monazite and xenotime analyses in gneiss sample RM-22-08 include propagated external uncertainties; age ranges (2σ) for monazite (m) and zircon (z) in the two granite samples reported by Mendum and Noble (2010) are also indicated. A time-averaged cooling rate of 50°C Ma^{-1} is indicated for the 12 Myr time period between the crystallization of monazite rims at 402 Ma and the deposition of unconformably overlying Middle Devonian (Eifelian) sediments at *c*. 390 Ma. Time-averaged cooling rates are also indicated for two combinations of limits of uncertainty in the monazite rim analyses and age limits of Eifelian; see the text for details. Crustal depths are inferred from deformation and crystallization temperatures, and assume a 30°C km^{-1} geotherm, with a corresponding time-averaged exhumation rate of 1.75 mm a^{-1} between 402 and 390 Ma; see the text for the discussion. Pr, Pragian. Source: the stratigraphic age ranges were taken from the 2023 update to the International Chronostratigraphic Chart (Cohen *et al*. 2013, updated 2023).

(Wellman 2015; Spencer *et al.* 2020 and references therein). Similarly, with the exception of the Rosemarkie Inlier, the oldest Devonian-age fluvial and lacustrine sedimentary rocks exposed along the east coast from Caithness southwards to Loch Ness (Meall Fuar-mhonaidh Outlier) are also of early–late Emsian age (Rogers *et al.* 1989, fig. 2; see also Marshall 2024, fig. 9.4). On the SE side of the fault zone, the oldest Devonian age sedimentary rocks traced from south to north are of late Emsian (Foyers area) to middle Eifelian (Inverness area) age (Rogers *et al.* 1989).

As noted above, only on the Rosemarkie Inlier (and the Cromarty Inlier immediately to the north: Fig. 2) do Devonian sedimentary rocks as young as middle–late Eifelian (*c.* 393–387 Ma) directly rest unconformably on basement rocks (Richardson 1960; Rogers *et al.* 1989; Fletcher *et al.* 1996; Marshall 2024). That said, on the north side of the Cromarty Firth (Fig. 3a) some of these rocks contain reworked Emsian palynomorphs, demonstrating that slightly older Lower Devonian sediments were originally deposited in this area (Marshall 2024, p. 272). The presence of Lower Devonian fluvial–lacustrine sedimentary basins along both the NW and SE sides of the GGFZ suggests that focused exhumation of the kilometre-wide sliver of mid-crustal Rosemarkie Inlier basement rocks during Emsian–Eifelian times (at a time-averaged exhumation rate of *c*. 1.75 mm a^{-1} between 402 and 390 Ma: Fig. 16) never resulted in significant topographical uplift, but rather that erosion essentially kept pace with rock uplift.

Fault-bounded slices of mylonite that formed during sinistral shearing have also been noted along two other structures thought to form part of the same network of late Caledonian faults. Watts *et al.* (2007) showed that mylonitization of basement gneisses along the Walls Boundary Fault (WBF) in Shetland (Fig. 1c) occurred at temperatures of 400–500°C, lower than at Rosemarkie. Thus far, no direct geochronological controls on the timing of shearing have been determined, although a late Caledonian age seems probable. Early sinistral shearing along the Møre–Trøndelag Fault Complex (MTFC) in Norway (Fig. 1c) has been constrained to 406 ± 11 Ma by $^{40}Ar/^{39}Ar$ dating of syndeformational muscovite within mylonites that formed at 300–500°C (Sherlock *et al.* 2004; Watts *et al.* 2023). Displacement on the MFTC therefore overlapped, within error, early Devonian sinistral shearing along the GGFZ, with the faults forming part of a network of overstepping sinistral strike-slip faults controlling Devonian extension and basin formation between Scotland and southern Norway (Fossen 2010, fig. 3). However, for neither the WBF nor the MTFC are there sufficient data to constrain the exhumation history with the same precision as achieved at Rosemarkie. Fossen and Dunlap (1998) have demonstrated that a rapid switch from orogenic contraction (convergence) to extension (divergence) occurred between 408 and 402 Ma in the Caledonides of southern Norway, with the western basement rocks cooling through *c*. 500°C at *c*. 404 Ma and 350°C shortly after (basement and lower nappes) during extensional top-to-the-NW transport of the orogenic wedge.

Summary and regional-scale correlations

The Rosemarkie Inlier, located on the NW side of the GGFZ at the SE edge of the NHT, comprises mylonitized, foliated and lineated Archean basement gneisses and Tonian (Moine) metasedimentary rocks in which the foliation strikes NE–SW (i.e. parallel to the GGFZ), dips steeply to the SE and contains a gently to moderately plunging mineral lineation. The lineation progressively changes from a NE to a SW plunge direction traced from the NE to the SW over a map distance of 8 km. Our microstructural, quartz *c*-axis fabric and petrochronology analyses are all based on samples collected from the NE end of this coastal section where the lineation plunges to the NE. The microstructural and quartz fabric studies indicate that the mineral lineation is orientated parallel to the maximum principal stretch direction (X), and that foliation/lineation developed during GGFZ-related oblique sinistral shearing and mylonitization under amphibolite-facies conditions. Deformation temperatures indicated by fabric opening angles in different samples range from *c*. 510 to 610°C, but well-developed GBM recrystallization microstructures between feldspar grains suggest that mylonitization may have started at higher temperatures. The gneisses and metasedimentary rocks are cut by a series of generally foliation sub-parallel granite sheets (Mendum and Noble 2010), which, at least locally, are also sinistrally sheared. Feldspar clasts in some of these granites have remained relatively rigid while the surrounding quartz grains have deformed plastically, indicating that the granites have been deformed at lower temperatures than the surrounding gneisses.

LA-ICP-MS analyses on monazite rims in gneiss sample RM-22-08 yielded a $^{206}Pb/^{238}U$ age of 401.8 ± 4.8 Ma (including 2σ uncertainty and a propagated additional 1% external uncertainty). A close similarity in deformation temperatures of 610°C indicated by quartz fabrics and 616 ± 25°C indicated by monazite–xenotime thermometry in adjacent gneiss samples RM-22-07 and RM-22-08 suggests that sinistral shearing was ongoing at *c*. 402 Ma. The granite sheets studied by Mendum and Noble (2010) had monazite and zircon crystallization ages of 397.6 ± 2.2 and 400.8 ± 2.6 Ma, respectively, and were sinistrally sheared at lower temperatures (<500°C) as indicated by the rigid/brittle nature of the feldspar

clasts. This suggests that the granite sheets were intruded slightly after the high-temperature (*c.* 600°C) shearing recorded in the surrounding gneisses, assuming that the granites essentially cooled instantaneously to the ambient deformation conditions.

The *c.* 402 Ma monazite rim age in the Rosemarkie Inlier gneisses is the youngest monazite age recorded in the NHT, and indicates that sinistral shearing and mylonitization at mid-crustal levels was ongoing within the GGFZ in Lower Devonian times when the Scandian thrust nappes of the NHT to the NW of the inlier had already been exhumed and Emsian (407–393 Ma) sediments deposited unconformably on top of them (Fig. 15). In contrast, the monazite cores that recorded temperatures greater than 650°C at 419 ± 5 Ma in the Rosemarkie Inlier gneisses are broadly consistent with the thermal structure of the Scandian hinterland recorded in the NHT thrust nappes (e.g. Thigpen *et al.* 2013; Mako *et al.* 2019). The Rosemarkie basement rocks are unconformably overlain by Middle Devonian (Eifelian, 393–387 Ma) sedimentary rocks, indicating time-averaged exhumation rates of *c.* 1.75 mm a^{-1} between 402 and *c.* 390 Ma, assuming a geothermal gradient of 30°C km^{-1}.

This time-averaged exhumation rate for the Rosemarkie Inlier may be compared with estimated exhumation rates for the earlier exhumed metamorphic rocks of the NHT to the NW (Fig. 15). For the Naver thrust sheet, Mako *et al.* (2019), using petrology-based pressure–temperature estimates and monazite–xenotime petrochronology, estimated time-averaged exhumation and cooling rates of 1.3–2.2 mm a^{-1} and 41–57°C Ma^{-1}, respectively, for the Lower Devonian time period between the initial retrograde metamorphism conditions of *c.* 600°C and 5–6 kb at *c.* 417.5 Ma and the deposition of overlying early Emsian sediments at 407–403 Ma. In contrast, a time-averaged exhumation/unroofing rate for the Naver thrust sheet of 1.0–1.4 mm a^{-1} between 425 Ma and Emsian times was estimated by Spencer *et al.* (2020), with corresponding time-averaged exhumation rates of 1.5–1.9 and 1.8–2.8 mm a^{-1} for the Ben Hope and Moine thrust sheets, respectively (Spencer *et al.* 2020; Thigpen *et al.* 2021). Bearing in mind that Scotland was located at *c.* 15° south of the equator in Silurian times (e.g. Cocks and Torsvik 2011), these time-averaged rates are comparable to present-day erosion rates in low-latitude (temperate to subtropical) active mountain belts dominated by fluvial erosion (Spencer *et al.* 2020). However, temperature–time paths based on $^{40}Ar/^{39}Ar$ thermochronology for the three thrust sheets suggest that exhumation rates in the NHT accelerated during the later stages of exhumation, possibly indicating the increasing importance of tectonic unroofing/normal faulting in Lower Devonian times (Spencer *et al.* 2020). This late-stage acceleration in exhumation rate could reflect an uptick in the rate of sinistral movements along the GGFZ and associated rifting along north–south normal faults seen in the Orcadian and Inner Moray Firth basins (e.g. Wilson *et al.* 2010; Dichiarante *et al.* 2020; Tamas *et al.* 2022) and all over the Northern and Central Highlands (e.g. Norton *et al.* 1987; Tamas *et al.* 2022).

More generally, the *c.* 407–393 Ma ages from the Rosemarkie Inlier for mid-crustal sinistral shearing and exhumation on the GGFZ fit remarkably well with both early sinistral shearing along the MTFC in the Norwegian Caledonides at 406 ± 11 Ma (Sherlock *et al.* 2004) and the timing of ductile extensional collapse in southern Norway at *c.* 402–394 Ma (Fossen and Dunlap 1998). This illustrates very well the regional importance of the GGFZ during sinistral transtensional deformation in the northern North Sea to western Norway regions (Fig. 1c) (e.g. Dewey and Strachan 2003; Fossen 2010; Wilson *et al.* 2010).

At present, we have no data to evaluate any possible connection between the arcuate doubly plunging lineation pattern recorded along the Rosemarkie coastal section and the exhumation of the basement rocks. Although this arcuate lineation pattern argues against the inclined transpression model proposed by Mendum and Noble (2010) for exhumation of the Rosemarkie Inlier, we argue that localization of young monazite crystallization ages on the SE margin of the NHT adjacent to the trace of the GGFZ suggests focused fault-driven exhumation from mid-crustal depths in Emsian–Eifelian times as broadly envisaged by Mendum and Noble (2010). The presence of Lower–Middle Devonian lacustrine sedimentary basins along both sides of the GGFZ suggests that exhumation of the kilometre-wide sliver of mid-crustal Rosemarkie Inlier basement rocks during Emsian–Eifelian times never resulted in significant topographical uplift, but rather that erosion essentially kept pace with rock uplift. Nonetheless, these are all continental strata and their elevation above sea level is not known. There could, therefore, have been some differential topographical uplift relative to the neighbouring end-Caledonian land surface.

Scientific editing by Dennis Newell

Acknowledgements We thank Rob Butler, Haakon Fossen and Kevin Mahan for their constructive and insightful reviews of an earlier version of the manuscript. We also thank Steve Noble for his helpful comments on the earlier manuscript and for cross-checking our isotopic age calculations. Tony Prave, Lee Watts and Alexandra Tamas are thanked for generously allowing us to use and modify the original digital versions of their published artwork in preparing Figures 1a, c and 2, respectively. Jim Spotila is thanked for discussion and advice on rates of exhumation on current and recently active strike-slip fault systems.

Author contributions **RDL**: conceptualization (lead), data curation (lead), formal analysis (lead), investigation (lead), methodology (lead), project administration (lead), validation (lead), visualization (lead), writing – original draft (lead), writing – review & editing (lead); **JRT**: conceptualization (equal), data curation (equal), formal analysis (equal), investigation (equal), visualization (equal), writing – original draft (equal), writing – review & editing (equal); **CAM**: conceptualization (equal), data curation (equal), formal analysis (equal), investigation (equal), visualization (equal), writing – original draft (equal), writing – review & editing (equal); **AK-C**: data curation (equal), investigation (equal), visualization (supporting), writing – review & editing (supporting); **MJC**: formal analysis (equal), investigation (equal), visualization (supporting), writing – original draft (supporting); **LRM**: formal analysis (equal), investigation (supporting); **CB**: investigation (equal), writing – review & editing (supporting); **REH**: conceptualization (equal), formal analysis (supporting), investigation (supporting), visualization (supporting), writing – original draft (equal), writing – review & editing (equal); **RAS**: conceptualization (equal), formal analysis (supporting), investigation (supporting), visualization (supporting), writing – original draft (equal), writing – review & editing (equal); **AGL**: conceptualization (supporting), formal analysis (supporting), investigation (supporting), visualization (supporting), writing – original draft (equal), writing – review & editing (equal).

Funding This research received no specific grant from any funding agency in the public, commercial, or not-for-profit sectors.

Competing interests The authors declare that they have no known competing financial interests or personal relationships that could have appeared to influence the work reported in this paper.

Data availability All data generated or analysed during this study are included in this published article (and its supplementary information file).

References

Aleinikoff, J.N., Schenck, W.S., Plank, M.O., Srogi, L.A., Fanning, C.M., Kamo, S.L. and Bosbyshell, H. 2006. Deciphering igneous and metamorphic events in high-grade rocks of the Wilmington Complex, Delaware; Morphology, cathodoluminescence and backscattered electron zoning, and SHRIMP U–Pb geochronology of zircon and monazite. *Geological Society of America Bulletin*, **118**, 39–64, https://doi.org/10.1130/B25659.1

Alsop, G.I. 1992. Late Caledonian sinistral strike-slip displacement across the Leannan Fault system, northwest Ireland. *Geological Journal*, **27**, 119–125, https://doi.org/10.1002/gj.3350270203

Andrews, I.J., Long, D., Richards, P.C., Thomson, A.R., Brown, S., Chesher, J.A. and McCormac, M. 1990. *The Geology of the Moray Firth*. British Geological Survey United Kingdom Offshore Regional Report. HMSO, London, https://webapps.bgs.ac.uk/data/publications/pubs.cfc?method=viewRecordandpublnId=19864776andseries=RGandsubseries=DN

Armitage, T.B., Watts, L.M., Holdsworth, R.E. and Strachan, R.A. 2021. Late Carboniferous dextral transpressional reactivation of the crustal-scale Walls Boundary Fault, Shetland: the role of preexisting structures and lithological heterogeneities. *Journal of the Geological Society, London*, **178**, https://doi.org/10.1144/jgs2020-078

Ashley, K.T., Thigpen, J.R. and Law, R.D. 2015. Prograde evolution of the Scottish Caledonides and tectonic implications. *Lithos*, **224–225**, 160–178, https://doi.org/10.1016/j.lithos.2015.03.011

Baden, C.W., Shuster, D.L., Hourigan, J.H., Golley, J.T., Cahill, M.R. and Hilley, G.E. 2024. Crustal block-controlled contrasts in deformation, uplift, and exhumation in the Santa Cruz Mountains, California, USA, imaged through apatite (U–Th)/He thermochronology and 3-D geological modelling. *Geological Society of America Bulletin*, **136**, 2789–2814, https://doi.org/10.1130/B36528.1

Becker, C. 2023. *Shearing on the Great Glen Fault: Kinematic and Microstructural Evidence Preserved at Different Crustal Levels*. MS thesis, Virginia Tech, Blacksburg, Virginia, USA, https://vtechworks.lib.vt.edu/items/bff5edcc-595d-4a7d-a008-019eab688178

Bird, A., Thirlwall, M., Strachan, R.A., Millar, I.L., Dempsey, E.D. and Hardman, K. 2023. Eclogites and basement terrane tectonics in the northern arm of the Grenville Orogen, NW Scotland. *Geosciences Frontiers*, **14**, https://doi.org/10.1016/j.gsf.2023.101668

Bird, T.J., Bell, A., Gibbs, A.D. and Nicholson, J. 1987. Aspects of strike-slip tectonics in the Inner Moray Firth Basin, offshore Scotland. *Norsk Geologisk Tidsskrift*, **67**, 353–369.

British Geological Survey 1958. *Nairn, Scotland Sheet 84, Solid Edition*. 1:50 000 Geology Series. British Geological Survey, Keyworth, Nottingham, UK.

British Geological Survey 1973. *Cromarty, Scotland Sheet 94, Solid Edition*. 1:50 000 Geology Series. British Geological Survey, Keyworth, Nottingham, UK.

British Geological Survey 1997. *Fortrose, Scotland Sheet 84W, Solid and Drift Edition*. 1:50 000 Geology Series. British Geological Survey, Keyworth, Nottingham, UK.

Cawood, P.A., Strachan, R.A. *et al.* 2015. Neoproterozoic to early Paleozoic extensional and compressional history of east Laurentian margin sequences: The Moine Supergroup, Scottish Caledonides. *Geological Society of America Bulletin*, **127**, 349–371, https://doi.org/10.1130/B31068.1

Cochran, W., Spotila, J.A., Prince, P.S. and McAleer, R.J. 2017. Rapid exhumation of Cretaceous arc-rocks along the Blue Mountains restraining bend of the Enriquillo–Plantain Garden fault, Jamaica, using thermochronology from multiple closure systems. *Tectonophysics*, **721**, 292–309, https://doi.org/10.1016/j.tecto.2017.09.021

Cocks, L.R.M. and Torsvik, T.H. 2011. The Palaeozoic geography of Laurentia and western Laurussia: A stable craton with mobile margins. *Earth-Science Reviews*, **106**, 1–51, https://doi.org/10.1016/j.earscirev.2011.01.007

Cohen, K.M., Finney, S.C., Gibbard, P.L. and Fan, J.X. 2013, updated 2023. The ICS International Chronostratigraphic Chart. *Episodes*, **36**, 199–204, https://stratigraphy.org/ICSchart/ChronostratChart2023-04.pdf

Dewey, J.F. and Ryan, P.D. 2022. Discussion of Searle, 'Tectonic evolution of the Caledonian orogeny in Scotland: a review based on the timing of magmatism, metamorphism and deformation'. *Geological Magazine*, **159**, 1833–1836, https://doi.org/10.1017/S0016756822000553

Dewey, J.F. and Strachan, R.A. 2003. Changing Silurian–Devonian relative plate motion in the Caledonides: sinistral transpression to sinistral transtension. *Journal of the Geological Society, London*, **160**, 219–229, https://doi.org/10.1144/0016-764902-085

Dewey, J.F., Dalziel, I.W.D., Reavy, R.J. and Strachan, R.A. 2015. The Neoproterozoic to Mid-Devonian evolution of Scotland: a review and unresolved issues. *Scottish Journal of Geology*, **51**, 5–30, https://doi.org/10.1144/sjg2014-007

Dichiarante, A.M., Holdsworth, R.E., Dempsey, E.D., McCaffrey, K.J.W. and Utley, T.A.G. 2020. Outcrop-scale manifestations of reactivation during multiple superimposed rifting and basin inversion events: the Devonian Orcadian Basin, northern Scotland. *Journal of the Geological Society, London*, **178**, https://doi.org/10.1144/jgs2020-089

Dumond, G., Mahan, K.H., Goncalves, P., Williams, M.L. and Jercinovic, M.J. 2022. Monazite as a monitor of shear strain in orogenic crust. *Journal of Structural Geology*, **161**, https://doi.org/10.1016/j.jsg.2022.104672

Faleiros, F.M., Moraes, R., Pavan, M. and Campanha, C. 2016. A new empirical calibration of the quartz c-axis opening-angle deformation thermometer. *Tectonophysics*, **671**, 173–182, https://doi.org/10.1016/j.tecto.2016.01.014

Fazio, E., Fiannacca, P., Russo, D. and Cirrincione, R. 2020. Submagmatic to solid-state deformation microstructures recorded in cooling granitoids during exhumation of Late-Variscan crust in North-East Sicily. *Geosciences*, **10**, https://doi.org/10.3390/geosciences10080311

Fettes, D.J., Long, C.B., Max, M.D. and Yardley, B.W.D. 1985. Grade and time of metamorphism in the Caledonian Orogen of Britain and Ireland. *Geological Society, London, Memoirs*, **9**, 41–53, https://doi.org/10.1144/GSL.MEM.1985.009.01.03

Fletcher, T.P., Auton, C.A., Highton, A.J., Merritt, J.W., Robertson, S. and Rollin, K.E. 1996. *Geology of the Fortrose and Eastern Inverness District. Memoir of the British Geological Survey Sheet 84W (Scotland)*. HMSO for the British Geological Survey, London.

Flinn, D. 1961. Continuation of the Great Glen Fault beyond the Moray Firth. *Nature*, **191**, 589–591, https://doi.org/10.1038/191589b0

Flinn, D. 1992. The history of the Walls Boundary fault, Shetland: the northward continuation of the Great Glen fault from Scotland. *Journal of the Geological Society, London*, **149**, 721–726, https://doi.org/10.1144/gsjgs.149.5.0721

Fossen, H. 2010. Extensional tectonics in the North Atlantic Caledonides. *Geological Society, London, Special Publications*, **335**, 767–793, https://doi.org/10.1144/SP335.31

Fossen, H. and Dunlap, W.J. 1998. Timing and kinematics of Caledonian thrusting and extensional collapse, southern Norway: Evidence from $^{40}Ar/^{39}Ar$ thermochronology. *Journal of Structural Geology*, **20**, 765–781, https://doi.org/10.1016/S0191-8141(98)00007-8

Harris, A.L. 1978. Metamorphic rocks of the Moray Firth District. *In:* Gill, G. (ed.) *The Moray Firth Area*. Inverness Field Club, Inverness, UK, 9–24.

Harris, A.L. 1995. The nature and timing of orogenesis in the Scottish Highlands and the role of the Great Glen Fault. *Geological Association of Canada Special Paper*, **41**, 65–79.

Heilbronner, R. and Tullis, J. 2006. Evolution of c-axis pole figures and grain size during dynamic recrystallization: results from experimentally sheared quartzite. *Journal of Geophysical Research: Solid Earth*, **111**, https://doi.org/10.1029/2005JB004194

Heinrich, W., Rehs, G. and Franz, G. 1997. Monazite–xenotime miscibility gap thermometry. I. An empirical calibration. *Journal of Metamorphic Geology*, **15**, 3–16, https://doi.org/10.1111/j.1525-1314.1997.t01-1-00052.x

Highton, A.J. 2009. Cromarty and Rosemarkie Inliers. *Geological Conservation Review Series*, **34**. Joint Nature Conservation Committee, Peterborough, UK, 458–464.

Holdsworth, R.E., Strachan, R.A. and Harris, A.L. 1994. Precambrian rocks in northern Scotland east of the Moine Thrust: the Moine Supergroup. *Geological Society, London, Special Reports*, **22**, 23–32, https://doi.org/10.1144/SR22.3

Holdsworth, R.E., Butler, C.A. and Roberts, A.M. 1997. The recognition of reactivation during continental deformation. *Journal of the Geological Society, London*, **154**, 73–78, https://doi.org/10.1144/gsjgs.154.1.0073

Holdsworth, R.E., Stewart, M., Imber, J. and Strachan, R.A. 2001. The structure and rheological evolution of reactivated continental fault zones: a review and case study. *Geological Society, London, Special Publications*, **184**, 115–137, https://doi.org/10.1144/GSL.SP.2001.184.01.07

Holdsworth, R.E., Selby, D., Dempsey, E., Scott, L., Hardman, K., Fallick, A.H. and Bullock, R. 2020. The nature and age of Mesoproterozoic strike-slip faulting based on Re–Os geochronology of syntectonic copper mineralization, Assynt Terrane, NW Scotland. *Journal of the Geological Society, London*, **177**, 686–699, https://doi.org/10.1144/jgs2020-011

Holgate, N. 1969. Palaeozoic and Tertiary transcurrent movements on the Great Glen Fault. *Scottish Journal of Geology*, **5**, 97–139, https://doi.org/10.1144/sjg05020097

Horne, J. 1923. *The Geology of the Lower Findhorn and Lower Strath Nairn, Including Part of the Black Isle Near Fortrose) with Contributions by B.N. Peach, L.W. Hinxman, R.G. Carruthers and E.M. Anderson and a Petographical Chapter by J.S. Flett). Memoir of the Geological Survey of Great Britain, Sheet 84 and Part of Sheet 94 (Scotland)*. HMSO, Edinburgh.

Horstwood, M.S.A., Košler, J. *et al.* 2016. Community-derived standards for LA-ICP-MS U–(Th–)Pb geochronology – uncertainty propagation, age interpretation and data reporting. *Geostandards and Geoanalytical Research*, **40**, 311–332, https://doi.org/10.1111/j.1751-908X.2016.00379.x

Imber, J., Holdsworth, R.E., Butler, C.A. and Strachan, R.A. 2001. A reappraisal of the Sibson–Scholz fault zone model: The nature of the frictional to viscous ('brittle–ductile') transition along a long-lived, crustal-scale fault, Outer Hebrides, Scotland. *Tectonics*, **20**, 601–624, https://doi.org/10.1029/2000TC001250

Kemp, S.J., Gillespie, M.R., Leslie, G.A., Zwingmann, H. and Campbell, S.D.G. 2019. Clay mineral dating of displacement on the Sronlairig Fault: implications for Mesozoic and Cenozoic tectonic evolution in northern Scotland. *Clay Minerals*, **54**, 181–196, https://doi.org/10.1180/clm.2019.25

Kennedy, W.Q. 1946. The Great Glen Fault. *Quarterly Journal of the Geological Society, London*, **102**, 41–76, https://doi.org/10.1144/GSL.JGS.1946.102.01-04.04

Krabbendam, M., Strachan, R. and Prave, T. 2022. Stratigraphic framework for early Neoproterozoic successions of Scotland. *Journal of the Geological Society, London*, **179**, https://doi.org/10.1144/jgs2021-054

Kylander-Clark, A.R.C. 2017. Petrochronology by laser-ablation inductively coupled plasma mass spectrometry. *Reviews in Mineralogy and Geochemistry*, **83**, 183–198, https://doi.org/10.2138/rmg.2017.83.6

Kylander-Clark, A.R.C., Hacker, B.R. and Cottle, J.M. 2013. Laser-ablation split-stream ICP petrochronology. *Chemical Geology*, **345**, 99–112, https://doi.org/10.1016/j.chemgeo.2013.02.019

Law, R.D. 2014. Deformation thermometry based on quartz crystal fabrics and recrystallization microstructures: A review. *Journal of Structural Geology*, **66**, 129–161, https://doi.org/10.1016/j.jsg.2014.05.023

Law, R.D., Strachan, R.A., Thirlwall, M.F. and Thigpen, J.R. 2024. The Caledonian orogeny: Late Ordovician to Early Devonian tectonic and magmatic events associated with closure of the Iapetus Ocean. *In*: Smith, M. and Strachan, R.A. (eds) *The Geology of Scotland*. 5th edn. Geological Society, London, 205–257, https://doi.org/10.1144/GOS5-2022-71

Lease, R.O., Haeussler, P.J., Witter, R.C., Stockli, D.F., Bender, A.M., Kelsey, H.M. and O'Sullivan, P.B. 2021. Extreme Quaternary plate boundary exhumation and strike slip localized along the southern Fairweather fault, Alaska, USA. *Geology*, **49**, 602–606, https://doi.org/10.1130/G48464.1

Le Breton, E., Cobbold, P.R. and Zanella, A. 2013. Cenozoic reactivation of the Great Glen fault, Scotland: additional evidence and possible causes. *Journal of the Geological Society, London*, **170**, 403–415, https://doi.org/10.1144/jgs2012-067

Leslie, G., Stone, P. and Strachan, R. 2024. Early–Middle Ordovician Grampian orogenesis: ophiolite obduction and arc–continent collision. *In*: Smith, M. and Strachan, R.A. (eds) *The Geology of Scotland*. 5th edn. Geological Society, London, 139–170, https://doi.org/10.1144/GOS5-2021-42

Lister, G.S. 1977. Discussion: Crossed-girdle c-axis fabrics in quartzites plastically deformed by plane strain and progressive simple shear. *Tectonophysics*, **39**, 51–54, https://doi.org/10.1016/0040-1951(77)90087-7

Lister, G.S. and Dornsiepen, U.F. 1982. Fabric transitions in the Saxony granulite terrain. *Journal of Structural Geology*, **4**, 81–92, https://doi.org/10.1016/0191-8141(82)90009-8

Lister, G.S. and Hobbs, B.E. 1980. The simulation of fabric development during plastic deformation of quartzite and its application to quartzite: The effect of deformation history. *Journal of Structural Geology*, **2**, 355–370, https://doi.org/10.1016/0191-8141(80)90023-1

Lister, G.S. and Snoke, A. 1984. S–C mylonites. *Journal of Structural Geology*, **6**, 617–638, https://doi.org/10.1016/0191-8141(84)90001-4

Lister, G.S., Paterson, M.S. and Hobbs, B.E. 1978. The simulation of fabric development in plastic deformation and its application to quartzite: The model. *Tectonophysics*, **45**, 107–158, https://doi.org/10.1016/0040-1951(78)90004-5

Mako, C.A. 2019. *Thermal and Metamorphic Evolution of the Northern Highlands Terrane, Scotland*. PhD thesis, Virginia Tech, Blacksburg, Virginia, USA, https://vtechworks.lib.vt.edu/handle/10919/90180

Mako, C.A., Law, R.D., Caddick, M.J., Thigpen, J.R., Ashley, K.T., Cottle, J. and Kylander-Clark, A. 2019. Thermal evolution of the Scandian hinterland, Naver nappe, northern Scotland. *Journal of the Geological Society, London*, **176**, 669–688, https://doi.org/10.1144/jgs2018-224

Mako, C.A., Caddick, M.J., Law, R.D. and Thigpen, J.R. 2024. Monazite–xenotime thermometry: a review of best practices and an example from the Caledonides of northern Scotland. *Geological Society, London, Special Publications*, **537**, 185–208, https://doi.org/10.1144/SP537-2022-246

Marshall, J.E.A. 2024. Old Red Sandstone: continental sedimentation on the eroding Caledonian Orogen. *In*: Smith, M. and Strachan, R.A. (eds) *The Geology of Scotland*. 5th edn. Geological Society, London, 259–292, https://doi.org/10.1144/GOS5-2022-43

Marshall, J.E.A., Astin, T.R., Brown, J.F., Mark-Kurik, E. and Lazauskiene, J. 2007. Recognizing the Kačák Event in the Devonian terrestrial environment and its implications for understanding land–sea interactions. *Geological Society, London, Special Publications*, **278**, 133–155, https://doi.org/10.1144/SP278.6

May, F., Highton, A.J., Clark, G.C. and Chacksfield, B.C. 1997. *Geology of the Invermoriston District. Memoir for 1:50 000 Geological Sheet 73W (Scotland)*. HMSO, London.

Mazza, S.E., Mako, C., Law, R.D., Caddick, M.J., Krabbendam, M. and Cottle, J. 2018. Thermobarometry of the Moine and Sgurr Beag thrust sheets, northern Scotland. *Journal of Structural Geology*, **113**, 10–32, https://doi.org/10.1016/j.jsg.2018.05.002

McBride, J.H. 1994. Investigating the crustal structure of a strike-slip 'step-over' zone along the Great Glen. *Tectonics*, **13**, 1550–1160, https://doi.org/10.1029/94TC00539

McGeary, S. 1989. Reflection seismic evidence for a Moho offset beneath the Walls Boundary strike-slip fault. *Journal of the Geological Society, London*, **146**, 261–269, https://doi.org/10.1144/gsjgs.146.2.0261

Mendum, J.R. and Noble, S.R. 2010. Mid-Devonian sinistral transcurrent movements on the Great Glen Fault: the rise of the Rosemarkie Inlier and the Acadian Event in Scotland. *Geological Society, London, Special Publications*, **335**, 161–187, https://doi.org/10.1144/SP335.8

Moser, A.C., Lusk, A.D., Attia, S., Garber, J.M., Seward, G.G.E. and Kylander-Clark, A.R.C. 2023. Titanite petrochronology records secular temperature and fluid evolution during ductile deformation: an example from Late Cretaceous shear zones in the Eastern Transverse Ranges. *Geochemistry, Geophysics, Geosystems*, **24**, https://doi.org/10.1029/2022GC010855

Mottram, C.M. and Cottle, J.M. 2024. An electron backscatter diffraction study of monazite: Linking the time–deformation path. *Chemical Geology*, **663**, https://doi.org/10.1016/j.chemgeo.2024.122238

Mykura, W. 1982. *The Old Red Sandstone East of Loch Ness, Inverness-shire*. Institute of Geological Sciences Report 82-13.

Norton, M.G., McClay, K.R. and Way, N.A. 1987. Tectonic evolution of Devonian basins in northern Scotland and southern Norway. *Norsk Geologisk Tidsskrift*, **67**, 323–338.

Palin, R.M., Searle, M.P. *et al.* 2013. A geochronological and petrological study of anatectic paragneiss and associated granite dykes from the Day Nui Con Voi metamorphic core complex, North Vietnam: constraints on the timing of metamorphism within the Red River shear zone. *Journal of Metamorphic Geology*, **31**, 359–387, https://doi.org/10.1111/jmg.12025

Passchier, C.W. and Trouw, R.A.J. 2005. *Microtectonics*. 2nd edn. Springer, New York.

Paton, C., Woodhead, J.D., Hellstrom, J.C., Hergt, J.C., Greig, A. and Maas, R. 2010. Improved laser ablation U–Pb zircon geochronology through robust downhole fractionation correction. *Geochemistry, Geophysics, Geosystems*, **11**, https://doi.org/10.1029/2009GC002618

Piasecki, M.A.J., van Breemen, O. and Wright, A.E. 1981. Late Precambrian geology of Scotland, England and Wales. *Canadian Society of Petroleum Geologists Memoirs*, **7**, 57–94, https://archives.datapages.com/data/cspg_sp/data/007/007001/57_cspgsp00700057.htm

Pitcher, W.S., Elwell, R.W.D., Tozer, C.F. and Cambray, F.W. 1964. The Leannan Fault. *Quarterly Journal of the Geological Society, London*, **120**, 241–273, https://doi.org/10.1144/gsjgs.120.1.0241

Prave, A.R., Stephens, W.E., Fallick, A.E., Williams, I. and Kirsimäe, K. 2024. How great is the Great Glen Fault? *Journal of the Geological Society, London*, **181**, https://doi.org/10.1144/jgs2024-085

Pyle, J.M., Spear, F.S., Rudnick, R.L. and Mcdonough, W.F. 2001. Monazite–xenotime–garnet equilibrium in metapelites and a new monazite–garnet thermometer. *Journal of Petrology*, **42**, 2083–2107, https://doi.org/10.1093/petrology/42.11.2083

Rathbone, P.A. and Harris, A.L. 1980. Moine and Lewisian near the Great Glen Fault in Easter Ross. *Scottish Journal of Geology*, **16**, 51–64, https://doi.org/10.1144/sjg16010051

Ribeiro, B.V., Kirkland, C.L. *et al.* 2023. Time–strain evolution of shear zones from petrographically constrained Rb–Sr muscovite analysis. *Earth and Planetary Science Letters*, **602**, https://doi.org/10.1016/j.epsl.2022.117969

Richardson, J.B. 1960. Spores from the Middle Old Red Sandstone of Cromarty, Scotland. *Palaeontology*, **3**, 43–63.

Roberts, N.M.W. and Holdsworth, R.E. 2022. Timescales of faulting through calcite geochronology: A review. *Journal of Structural Geology*, **158**, https://doi.org/10.1016/j.jsg.2022.104578

Rogers, D.A., Marshall, J.E.A. and Austin, T.R. 1989. Devonian and later movements on the Great Glen fault system, Scotland. *Journal of the Geological Society, London*, **146**, 369–372, https://doi.org/10.1144/gsjgs.146.3.0369

Schmid, S.M. and Handy, M.R. 1991. Towards a genetic classification of fault rocks: geological usage and tectonophysical implications. *In*: Muller, D.W., McKenzie, J. and Weissert, H. (eds) *Controversies in Modern Geology*. Academic Press, New York, 339–361.

Searle, M.P. 2021. Tectonic evolution of the Caledonian orogeny in Scotland: a review based on the timing of magmatism, metamorphism and deformation. *Geological Magazine*, **159**, 124–152, https://doi.org/10.1017/S0016756821000947

Sherlock, S.C., Watts, L.M., Holdsworth, R.E. and Roberts, D. 2004. Dating fault reactivation by Ar/Ar laserprobe: an alternative view of apparently cogenetic mylonite–pseudotachylite assemblages. *Journal of the Geological Society, London*, **161**, 335–338, https://doi.org/10.1144/0016-764903-160

Sibson, R.H. 1977. Fault rocks and fault mechanisms. *Journal of the Geological Society, London*, **133**, 191–213, https://doi.org/10.1144/gsjgs.133.3.0191

Smith, D.I. and Watson, J. 1983. Scale and timing of movements on the Great Glen fault, Scotland. *Geology*, **11**, 523–526, https://doi.org/10.1130/0091-7613(1983)11<523:SATOMO>2.0.CO;2

Snoke, A.W. and Tullis, J. 1998. An overview of fault rocks. *In*: Snoke, A.W., Tullis, J. and Todd, V.R. (eds) *Fault-Related Rocks: A Photographic Atlas*. Princeton University Press, Princeton, NJ, 3–18.

Spencer, B.M., Thigpen, J.R., Law, R.D., Mako, C., McDonald, C.S., Hodges, K.V. and Ashley, K.T. 2020. Rapid cooling during late stage orogenesis and implications for collapse of the Scandian retrowedge, northern Scotland. *Journal of the Geological Society, London*, **177**, https://doi.org/10.1144/jgs2020-022

Spencer, B.M., Thigpen, J.R., Gallen, S.F., Dortch, J.M., Hodges, K.V., Law, R.D. and Mako, C.M. 2021. An evaluation of erosional–geodynamic thresholds for rapid orogenic denudation. *Journal of Geophysical Research: Solid Earth*, **126**, e2021JB022353, https://doi.org/10.1029/2021JB022353

Spotila, J.A., Farley, K.A., Yule, J.D. and Reiners, P.W. 2001. Near-field transpressive deformation along the San Andreas fault zone in southern California, based on exhumation constrained by (U–Th)/He dating. *Journal of Geophysical Research*, **106**, 30 909–30 922, https://doi.org/10.1029/2001JB000348

Stewart, M. 2010. Excursion 14 – Great Glen. *In*: Strachan, R.A., Alsop, I., Friend, C.R.L. and Miller, S. (eds) *An Excursion Guide to the Moine Geology of the Northern Highlands of Scotland*. Edinburgh Geological Society and Geological Society of Glasgow, Edinburgh, 266–281.

Stewart, M., Strachan, R.A. and Holdsworth, R.E. 1997. Direct field evidence for sinistral displacements along the Great Glen Fault Zone: Late Caledonian reactivation of a regional basement structure? *Journal of the Geological Society, London*, **154**, 135–139, https://doi.org/10.1144/gsjgs.154.1.0135

Stewart, M., Strachan, R.A. and Holdsworth, R.E. 1999. Structure and early kinematic history of the Great Glen Fault Zone, Scotland. *Tectonics*, **18**, 326–342, https://doi.org/10.1029/1998TC900033

Stewart, M., Holdsworth, R.E. and Strachan, R.A. 2000. Fault-rock evolution during early movements along the Great Glen Fault Zone, Scotland: An insight into deformation processes in the frictional- to viscous-creep transition zone. *Journal of Structural Geology*, **22**, 543–560, https://doi.org/10.1016/S0191-8141(99)00164-9

Stewart, M., Strachan, R.A., Martin, M.W. and Holdsworth, R.E. 2001. Dating early sinistral displacements along the Great Glen Fault Zone, Scotland: structural setting, emplacement and U–Pb geochronology of the syn-tectonic Clunes Tonalite. *Journal of the Geological Society, London*, **158**, 821–830, https://doi.org/10.1144/jgs.158.5.821

Stoker, M.S. 1982. Old Red Sandstone sedimentation and deformation in the Great Glen fault Zone, NW of Loch Linnhe. *Scottish Journal of Geology*, **18**, 147–156, https://doi.org/10.1144/sjg18020147

Strachan, R.A., Harris, A.L., Fettes, D.J. and Smith, M. 2002. The Highland and Grampian terranes. *In*: Trewin, N.H. (ed.) *The Geology of Scotland*. 4th edn. Geological Society, London, 81–148.

Strachan, R.A., Alsop, G.I., Ramezani, J., Frazer, R.E., Burns, I.M. and Holdsworth, R.E. 2020. Patterns of Silurian deformation and magmatism during sinistral oblique convergence, northern Scottish Caledonides. *Journal of the Geological Society, London*, **177**, 893–910, https://doi.org/10.1144/jgs2020-039

Strachan, R.A., Prave, T., Krabbendam, M. and Smith, M. 2024. Late Mesoproterozoic–middle Neoproterozoic: sedimentation and orogeny on the margin of Rodinia. *In*: Smith, M. and Strachan, R.A. (eds) *The Geology of Scotland*. 5th edn. Geological Society, London, 81–110, https://doi.org/10.1144/GOS5-2022-14

Tamas, A., Holdsworth, R.E. *et al.* 2022. New onshore insights into the role of structural inheritance during Mesozoic opening of the Inner Moray Firth Basin, Scotland. *Journal of the Geological Society, London*, **179**, https://doi.org/10.1144/jgs2021-066

Tamas, A., Holdsworth, R.E. *et al.* 2023. Older than you think: using U–Pb calcite geochronology to better constrain basin-bounding fault reactivation, Inner Moray Firth Basin, western North Sea. *Journal of the Geological Society, London*, **180**, https://doi.org/10.1144/jgs2022-166

ten Grotenhuis, S.M., Trouw, R.A.J. and Passchier, C.W. 2003. Evolution of mica fish in mylonitic rocks. *Tectonophysics*, **372**, 1–21, https://doi.org/10.1016/S0040-1951(03)00231-2

Thigpen, J.R., Law, R.D. *et al.* 2013. Thermal structure and tectonic evolution of the Scandian orogenic wedge, Scottish Caledonides: integrating geothermometry, deformation temperatures and conceptual kinematic–thermal models. *Journal of Metamorphic Geology*, **31**, 813–842, https://doi.org/10.1111/jmg.12046

Thigpen, J.R., Ashley, K.T., Mako, C., Law, R.D. and Spencer, B. 2021. Interplay between crustal-scale thrusting, high metamorphic heating rates and the development of inverted thermal metamorphic gradients: numerical models and examples from the Caledonides of northern Scotland. *Tectonics*, **40**, https://doi.org/10.1029/2021TC006716

Thomson, K. and Underhill, J.R. 1993. Controls on the development and evolution of structural styles in the Inner Moray Firth Basin. *Geological Society, London, Petroleum Geology Conference Series*, **4**, 1167–1178, https://doi.org/10.1144/0041167

Tomascak, P.B., Krogstad, E.J. and Walker, R.J. 1996. U–Pb monazite geochronology of granitic rocks from Maine; Implications for late Paleozoic tectonics in the Northern Appalachians. *Journal of Geology*, **104**, 185–195, https://doi.org/10.1086/629813

Tullis, J. 1977. Preferred orientation of quartz produced by slip during plane strain. *Tectonophysics*, **39**, 87–102, https://doi.org/10.1016/0040-1951(77)90090-7

Tullis, J. 2002. Deformation of granitic rocks: experimental studies and natural examples. *Reviews in Mineralogy and Geochemistry*, **51**, 51–95, https://doi.org/10.2138/gsrmg.51.1.51

Underhill, J.R. 1991. Implications of Mesozoic – recent basin development in the Western Inner Moray Firth. *Journal of Marine and Petroleum Geology*, **8**, 359–369, https://doi.org/10.1016/0264-8172(91)90089-J

Underhill, J.R. and Brodie, J.A. 1993. Geology of Easter Ross, Scotland: implications for movement on the Great Glen fault zone. *Journal of the Geological Society, London*, **150**, 515–527, https://doi.org/10.1144/gsjgs.150.3.0515

Watts, L.M., Holdsworth, R.E., Sleight, J.A., Strachan, R.A. and Smith, S.A.F. 2007. The movement history and fault rock evolution of a reactivated crustal-scale strike-slip fault: the Walls Boundary Fault Zone, Shetland. *Journal of the Geological Society, London*, **164**, 1037–1058, https://doi.org/10.1144/0016-76492006-156

Watts, L.M., Holdsworth, R.E., Roberts, D., Sleight, J.M. and Walker, R.J. 2023. Structural evolution of the reactivated Møre–Trøndelag Fault Complex, Fosen Peninsula, Norway. *Journal of the Geological Society, London*, **180**, https://doi.org/10.1144/jgs2022-139

Wellman, C.H. 2015. Spore assemblages from the Lower Devonian 'Lower Old Red Sandstone' deposits of the Northern Highlands of Scotland: the Berriedale Outlier. *Earth and Environmental Science Transactions of the Royal Society of Edinburgh*, **105**, 227–238, https://doi.org/10.1017/S1755691015000055

Williams, M.L. and Jercinovic, M.J. 2002. Microprobe monazite geochronology: Putting absolute time into microstructural analysis. *Journal of Structural Geology*, **24**, 1013–1028, https://doi.org/10.1016/S0191-8141(01)00088-8

Williams, M.L., Jercinovic, M.J. and Hetherington, C.J. 2007. Microprobe monazite geochronology: understanding geologic process by integrating composition and chronology. *Annual Review of Earth and Planetary Sciences*, **35**, 135–175, https://doi.org/10.1146/annurev.earth.35.031306.140228

Williams, M.L., Jercinovic, M.J., Mahan, K.H. and Dumond, G. 2017. Electron microprobe petrochronology. *Reviews in Mineralogy and Geochemistry*, **83**, 153–182, https://doi.org/10.2138/rmg.2017.83.5

Wilson, J.T. 1962. Cabot Fault, an Appalachian equivalent of the San Andreas and Great Glen faults and some implications for continental displacement. *Nature*, **195**, 135–138, https://doi.org/10.1038/195135a0

Wilson, R.W., Holdsworth, R.E., Wild, L.E., McCaffrey, K.J.W., England, R.W., Imber, J. and Strachan, R.A. 2010. Basement-influenced rifting and basin development: a reappraisal of post-Caledonian faulting patterns from the North Coast Transfer Zone, Scotland. *Geological Society, London, Special Publications*, **335**, 795–826, https://doi.org/10.1144/SP335.32

Winchester, J.A. 1973. Pattern of regional metamorphism suggests a sinistral displacement of 160 km along the Great Glen Fault. *Nature*, **246**, 81–84, https://doi.org/10.1038/physci246081a0